Title: Microbiome disturbance and resilience dynamics of the upper respiratory tract in response to influenza A virus infection in humans and ferrets

Authors: Drishti Kaul[1,8], Raveen Rathnasinghe[2,8], Marcela Ferres[2], Gene S. Tan[1,3], Aldo Barrera[2,4], Brett E. Pickett[5], Barbara A. Methe[5a], Suman Das[5], Isolda Budnik[2], Rebecca A. Halpin[5], David Wentworth[5b], Mirco Schmolke[6c], Ignacio Mena[6], Randy A. Albrecht[6], Indresh Singh[5], Karen E. Nelson[5], Adolfo García-Sastre[6,7], Chris L. Dupont[1*], Rafael A. Medina[2,4,6*].

Affiliations:

[1]J. Craig Venter Institute, 4120 Capricorn Lane, La Jolla, CA 92037, USA.

[2]Departmento de Enfermedades Infecciosas e Inmunología Pediátrica, Facultad de Medicina, Pontificia Universidad Católica de Chile, Santiago, Chile.

[3] Department of Infectious Diseases, University of California San Diego, La Jolla, CA 92037, USA

[4]Millennium Institute on Immunology and Immunotherapy, Santiago, Chile

[5]J. Craig Venter Institute, 9704 Medical Center Drive, Rockville, Maryland 20850, 14 USA.

[6]Department of Microbiology, Global Health and Emerging Pathogens Institute, Icahn School of Medicine at Mount Sinai, New York, NY 10029, USA.

[7]Department of Medicine, Icahn School of Medicine at Mount Sinai, New York, NY 10029, USA.

[8]These authors contributed equally to this work

[a] University of Pittsburgh, Department of Medicine, Pittsburgh PA 15213

[b] Present address: National Center for Immunization and Respiratory Diseases, Centers for Disease Control and Prevention, Atlanta, GA, USA.

[c] Present address: Department of Microbiology and Molecular Medicine, University of Geneva, Switzerland

*Corresponding author: E-mail: rmedinas@med.puc.cl (Lead Contact), cdupont@jcvi.org

One Sentence Summary: Dynamics of the upper respiratory tract microbiome during influenza A virus infection

Abstract:

Infection with influenza can be aggravated by bacterial co-infections, which often results in disease exacerbation because of host responses and cellular damage. The native upper respiratory tract (URT) microbiome likely plays a role, yet the effects of influenza infection on the URT microbiome are largely unknown. We performed a longitudinal study to assess the temporal dynamics of the URT microbiomes of uninfected and influenza virus-infected humans and ferrets. Uninfected human patients and ferret URT microbiomes had stable “heathy ecostate” communities both within and between individuals. In contrast, infected patients and ferrets

exhibited large changes in bacterial community composition over time and between individuals. The “unhealthy” ecostates of infected individuals progressed towards the “healthy ecostate” over time, coinciding with viral clearance and recovery. Blooms of *Pseudomonas* were a statistically associated constant in the disturbed microbiomes of infected individuals. The dynamic and resilient nature of the microbiome during influenza virus infection in multiple hosts provides a compelling rationale for the maintenance of the microbiome homeostasis as a potential therapeutic target to prevent IAV associated bacterial co-infections.

Keywords: Influenza A virus, resilience, biodiversity, microbiome, upper respiratory tract, H1N1, H3N2, ecostate, humans, ferrets

Main Text:

Introduction

Influenza A virus (IAV) is a highly infectious upper respiratory tract (URT) disease in humans and animals caused by a negative-sense segmented RNA virus. It is recognized as a major public health concern resulting yearly in significant disease and economic burden. Frequent nucleotide substitutions lead to changes on the hemagglutinin and neuraminidase glycoproteins on the surface of IAV particles (also known as antigenic drift) that contribute to the need for continuous vaccine updates. This evolutionary arms race between vaccine design and viral mutation contributes to annual influenza epidemics worldwide, which on average results in 3 to 5 million cases of severe illness and up to 291,000 to 646,000 deaths annually (*1*). The modular architecture of the segmented IAV genome allows for genetic re-assortment (antigenic shift) with other divergent IAVs, resulting in the sporadic emergence of novel viruses capable of causing large epidemics or pandemics. Circulation of a new IAV in the naïve human population has

caused pandemics in the past resulting in significant morbidity and mortality, the most notable in 1918 and 1919, when the *Spanish flu* killed approximately 20 to 50 million people worldwide (*2*). Retrospective analyses of autopsy specimens from the 1918 pandemic revealed the prevalence of secondary superinfection caused by URT bacteria (*3-5*). However, the role of bacterial co-infection in disease prognosis is not only confined to pandemics; bacterial and virus co-infection during seasonal influenza epidemics are commonly associated with increase hospital admissions, severe disease and deaths (*6, 7*).

Although the microbiome of non-diseased individuals is relatively stable, IAV infection has been shown to increase the diversity of bacterial taxa that are present in the URT (*8*). Specifically, IAV can cause changes in the relative abundances of *Staphylococcus* and *Bacteroides* genera (*9*), as well as *Haemophilus*, *Fusobacteria*, and other taxa (*10*). Temporary disturbances to the microbiome due to the changes in the local epithelia during acute or chronic conditions has also been reported as a predisposing factor for infections (*11-14*). The observed diversity in the human URT microbiome, together with its role in immunity and susceptibility to pathogens has been described previously (*11, 15, 16*). Other studies have reported that the URT microbiome may also play a beneficial role in modulating the inflammatory response induced during IAV infection (*16, 17*). In addition, the intestinal microbiome composition has been shown to positively regulate the toll-like receptor 7 signaling pathway following infection with IAV (*18*). Nonetheless, the exact mechanisms by which prior infection with IAV increase susceptibility to a secondary bacterial infection have not been determined. Importantly, the effect of IAV replication and induction of innate immune response on the composition of the human or animal URT microbiome remains to be elucidated and analyzed in depth on a community wide scale.

Humans and ferrets share similar lung physiology and both are known to be susceptible and transmit the same strains of the IAVs (*19, 20*). This has made the ferrets an ideal model to study the dynamics of IAV infection in URT. However, it is unknown whether there is similarity between the ferret and human URT microbiome in terms of composition and its temporal dynamics and modulation upon IAV infection. In this study, we examined the longitudinal diversity of the URT microbiome of influenza infected and uninfected human cohorts, as well as control uninfected and experimentally infected ferrets. These experiments revealed a strong consistency in the microbiome composition and dynamics between the two host systems, demonstrating that experimentally infected ferrets recapitulated closely the modulation of the microbiome observed in naturally infected humans. Our results suggest that microbiome disturbance and resilience dynamics may be critical to addressing the bacterial co-infections associated with influenza-derived morbidity.

Results

Effects of influenza on the URT microbiome dynamics in human clinical samples

In order to determine if the human microbiome structure is modulated by the IAV infection, we established a human cohort study and obtained nasopharyngeal swabs at multiple time points after the initial influenza-prompted hospital visits (days 1 to 22) from 30 human subjects recruited during 2011 and 2012. As healthy controls, we included nasal swab samples taken at 6 time points (days 1, 2, 3, 5, 7 and 28) from 22 healthy human subjects free of any respiratory infections (Table S1). Our goal was to assess and compare the temporal microbiome biodiversity in response to ecological disturbances of the URT caused by viral infection.

The dynamics and relative abundances of bacteria in the URT microbiome were examined by pyrosequencing of the V1-V3 region of the 16S rRNA, which yielded a total of 2.3 million sequences, which clustered into 707 operational taxonomic units (OTUs) (Table 1). The count abundance data for the OTUs was normalized to account for the sampling process and the library size, as confounding factors for the beta-diversity analyses. Additionally, OTUs with counts less than 5 were removed to avoid inflating the importance of any contaminant sequences that might be present in the data. This resulted in over 90% of the reads mapped back to the OTUs (Table 1). Metric multidimensional scaling of the beta diversity explains 38.5% of the variability across the first three components (Fig. 1). The plot shows that the IAV infection status has a strong influence on the ordination of the samples, as measured by the Bray-Curtis metric ($R=0.649$, p-value < 0.001). The uninfected and infected communities cluster away from each other (Fig. 1). Of interest, the microbiome for the IAV-infected cohort is more dynamic than that of the uninfected IAV-free cohort, validating the "Anna Karenina" principle of microbiomes, which refers to the notion that there is much more variability in the microbial communities of infected (dysbiotic) individuals than in healthy individuals. The nasopharyngeal samples from infected humans demonstrated higher diversity between infection states than within them (Fig. S1). The t-statistic for the "All within infection" versus "All between infection" for the human data set was -150.82 and the p-value was also significant (Table S2), which indicates that IAV infection in humans results in the clustering of microbiomes according to infection status.

Perturbation and resilience of the human URT microbiome is not dependent on the clinical parameters or influenza virus subtype

To complement the qualitative overview of the IAV-infected data points, we integrated additional clinical metadata including gender, antibiotic usage, age and influenza subtype; and included details of the amplification of IAV genomes from these samples to more accurately classify these data points as either positive or unknown for the presence of virus. Positive and unknown infected microbiomes were tested to determine if they were distinct enough to cluster separately based on their beta diversity. Analyses of the beta diversity metrics using PCoA, focusing just on the IAV-infected samples, did not allow deriving any conclusions from this analysis alone. In addition, the grouping of infected samples based on gender did not show any significant association (ANOSIM R=0.03124, p-value <0.023), implying that there was no significant effect of gender on the clustering of the samples (Table S3). When we used distances between the samples as the response variable (ADONIS *df* 1, R^2 =0.0209), only 2.1% of the variation in the distances was explained when the gender of the patients was accounted for as a predictor of the model. Hence, sex could not be correlated with the microbiome of the infected human samples. Age and effects of post visit antibiotic treatment on the microbiome trends were also examined. No significant association could be observed between post visit antibiotic usage and clustering of the infected human samples in two statistical tests (ANOSIM R=-0.046, p-value < 0.732, and ADONIS *df* 1, R^2 =0.012), which was surprising. However, the age of the patients seemed to have some influence on the sample grouping when all 26 categorical values were taken into consideration (ANOSIM R=0.47, p-value < 0.001). The statistical analyses show that while the p-value was significant, the clustering on the basis of age was only moderately strong (ADONIS R^2 = 0.409, *df* 25; Table S3). Since there was no indication of this effect among IAV-infected patients in the ordination plots, it is possible that the significant p-value could be attributed to the high number of samples or the differences in dispersion among the different

sample groupings, emphasizing the importance of considering in the analysis both the p-value and the effect size.

Pseudomonas blooms during viral infection in the human URT

We examined taxonomic profiles for all the infected and healthy patients across all the time points using the taxa abundance values for the top ten most prevalent taxa at the order level (Fig. 2). All other taxa were pooled into an additional taxon named "Other". *Pseudomonas* was the most abundant taxonomic group in all samples from influenza-infected individuals (Fig. 2, and Fig. S2 and S3). Less abundant phyla included *Bacteroidetes*, *Firmicutes*, *Actinobacteria* and some other families of *Proteobacteria*, like Rhodanobactere*ceae* and *Pasteurellaceae* (c. *Gammaproteobacteria*) and *Brucellaceae* of the *Rhizobiales* order (c. *Alphaproteobacteria*). *Pseudomonas* was also clearly identified as the predominant taxon when temporal dynamic analyses were done on individuals independently (Fig. S4). As for the uninfected subjects, *Actinobacteria* was the most dominant taxon and *Pseudomonas* was the least abundant taxonomic group present, also seen when individual subjects where analyzed (Fig. S4). Other less abundant phyla included *Verrucomicrobia* and within the *Proteobacteria*, the *Alphaproteobacteria* and *Epsilonproteobacteria* classes.

The human URT microbiome is distributed into distinct ecostates due to IAV infection

Due to the dynamic nature of the human URT microbiome during IAV infection, we hypothesized that infection perturbs the microbiome structure resulting in distinct signature microbiomes that differentiate infected from uninfected individuals. Thus, we used the Infinite Dirichlet-multinomial Mixture Model (iDMM) (*21*), which is an extension of the Dirichlet-multinomial mixture model (DMM) (*22*) that helps understand and interpret taxon abundance

data by adding statistical validation if a taxa is associated with a given case-control condition. This is an un-supervised clustering method that applies Bayesian statistics to quantitatively assess the data and accurately capture the features that are present. Essentially, given a set of subsampled distributions, the iDMM model predicts the original number of full-size distributions together with their composition. The nonparametric nature of the iDMM model makes it ideal for understanding the complex ecological data in this study, where the original number of the sampled communities (known as ecostates) is unknown.

The iDMM model was run over 2000 iterations over all data points (33 patients at multiple time points), which collapsed the data into a total of four ecostates (Table 2). Plotting the mean of the likelihood ratio at each iteration showed that, 25 iterations into the analysis, the maximum likelihood ratio converges for the model. One of the four ecostates included all 127 uninfected data points (or the "healthy" ecostate) while the 146 infected data points were distributed across the three other ecostates (or "unhealthy" ecostates). Interestingly, a few patients moved from the "unhealthy" ecostates during acute influenza infection to the "healthy" ecostate in the later time points. This suggests that the human microbiome exhibits resilience but potentially a weak elasticity; however, this could be due to the lack of a precise temporal control of the time of infection.

We also identified a diagnostic OTU for each of these ecostates, which is the OTU with the highest posterior predictive probability in the ecostate and therefore drives the clustering. The iDMM analysis predicted the diagnostic OTU for the healthy ecostate to be Otu000008 which belongs to the *Flavobacteria* class (*Cloacibacterium*), with a posterior predictive probability of 0.08, followed by Otu000010 (Corynebacterium_1) and Otu000013 (*Comamonadaceae*), belonging to the class Actinobacteria and Betaproteobacteria, respectively (Table 2). For the

"unhealthy" ecostates, Otu000003, Otu000004 and Otu000002 were diagnostic for Ecostate 1, 2 and 3 respectively (Table 2). Ecostate 1 had the largest number of infected data points (114), followed by Ecostate 3 (20) and Ecostate 2 (9). Otu000003 and Otu000002 belong to the *Pseudomonadaceae* family (the latter being an unclassified *Pseudomonadaceae*), with relatively high posterior probabilities associated with each of them (Table 2). Otu000004 belonged to the *Actinobacteria* class and was the diagnostic OTU for Ecostate 2 with 9 infected data points. Remarkably, the diagnostic OTUs for all four ecostates for the human samples are also among the first ten most abundant OTUs for the data.

A random forest analysis was also used to identify predictive features in the data. The method we developed iterates through unique random forest models (each seeded with a different random state) and attempts to fit the model to a random subset of the data with five samples removed from the training set, (see Materials and Methods). If the model could accurately predict all five of the omitted samples during the cross-validation step, then its feature importance vector (mean decrease gini index) including weights for every OTU's predictive capacity was collected. The results from the random forest classification aligned with our diagnostic iDMM OTU prediction in the human samples (Table S4). The analysis showed Otu000002 (unclassified *Pseudomonadales*) to be the most predictive of the IAV-infected samples, followed by Otu000001 (*Rhizobiales*) and Otu000003 (*Pseudomonas*) with a maximum accuracy of 71%. When we examined the taxonomy of Otu000001 in detail, it was classified with 100% confidence down to Genus Ochrobactrum, at which point the read length is unable to differentiate the species any further. Nevertheless, the actual OTU sequence is 100% identical to Ochrobactum anthropi, an opportunistic human pathogen (*23-25*). Similarly, the in depth analyzes of Otu000006 identified the taxonomy of this OTU as uncultivated lineages of

Rhodanobacter, which have also been previously associated with human respiratory tract microbiomes (*26*). Comparison with our negative controls confirmed that these were not contaminants and supported the notion that Ochrobactrum was also diagnostic for the infection state in humans, which is likely to be consistent with the presence of *O. anthropii* or similar opportunistic species.

Influenza virus infection modulates the microbiome structure of the URT in ferrets

We hypothesized that IAV infection in ferrets will result in the clustering of microbiomes according to infection status, as observed during IAV infection in humans. Therefore, using the well-established ferret model of IAV infection, we designed a longitudinal study resembling the clinical specimens obtained from human patients to obtain nasal wash samples from infected animals. We collect nasal washes from 7 uninfected ferrets and 7 ferrets infected with the A/Netherlands/602/2009 (H1N1) pandemic strain, at 0, 1, 3, 5, 7 and 14 days post infection (dpi). The dynamics and relative abundances of bacteria in the URT microbiome were examined by pyrosequencing of the V1-V3 region of the 16S rRNA using similar thresholds for length and expected error as were chosen for the human data. A total of 649,440 reads clustered into 259 (OTUs) with 79% of reads mapping (Table 1). As before, the count abundance data for the OTUs was normalized and the low abundance taxa were filtered out from the count data. Principal Coordinates Analysis (PCoA) of beta diversity between the healthy and IAV infected groups demonstrated variability consistent with the virus perturbing and modulating the microbiome structure (Fig. 3). Infection status strongly influenced the ordination of the samples as measured by the Bray-Curtis beta-diversity metric ($R=0.503$, p-value < 0.001). The IAV-negative and IAV-positive ferret microbial communities formed discrete clusters, while samples from the IAV

infected animals showed divergence from each other (Fig. 3). By the final time point, day 14, the microbiome of infected ferrets (light blue) was more similar to the Day 0 samples (lavender) and those of the uninfected controls (dark blue).

Quantitative metrics of diversity were used to compare the microbiomes of influenza infected and control ferrets. Beta diversity distance analyses (Fig. S5) demonstrated that ferret microbiomes had higher diversity between infection states than within them. Student's two sample two-sided t-tests confirmed that the diversity between the two states (infected and uninfected) was statistically significant, with the microbiomes of infected ferrets being more diverse (Table S5). The t-statistic for the "All within infection" versus "All between infection" was -29.1592 corresponding to a Bonferroni-corrected parametric p-value of 1.90e-166 (Table S5). The PCoA and statistical analyses showed that infected ferrets have a far more dynamic URT microbiome than that of the uninfected group. We note that the "healthy" baseline experiments were not conducted at the same time and some divergence of the microbiomes was expected given the high level of personalization, and that ferrets are outbred. Remarkably, 4/7 T=0 time points and 7/7 t=14 time points converged to the "healthy" microbiome from an independent experiment. Overall, the quantitative examination revealed that the range for infection-associated beta diversity was much lower in the ferret samples than it was from human clinical samples.

IAV infection induces temporal changes in the structure of the ferret URT microbiome

To assess the correlation of clinical symptoms overtime during acute IAV infection, we monitored the body weight of all ferrets from 0 to 14 dpi, which demonstrated a clear weight loss

among the infected animals (Fig. 4A). As expected, the maximum weight loss coincided with peak IAV titer from 3 to 5 dpi, and recovery in body weight correlated with the lack of detectable virus after day 7 (Fig. 4B). To better visualize the temporal trajectory of the ferret microbiome, the community composition for one representative influenza-infected and one uninfected ferret (ferret_595 and ferret_592, respectively) were examined with regards to their taxonomic profiles across six different time points (Fig. 4C and 4D). At the order level, the IAV-infected ferrets exhibited *Pseudomonadales* abundance at days 5 and 7 dpi (Fig. 4C-F), which correlated with maximal weight loss and peak viral titers (Fig. 4A and B), suggesting the direct or indirect influence of the infection on the microbiome. A few of the less-abundant phyla included *Actinobacteria* and *Firmicutes* (Fig. S6). The abundance of *Pseudomonas* decreased over time in the infected ferrets, reaching the basal abundance found in healthy ferrets 14 dpi. For the uninfected ferrets, the microbiomes were more stable and *Clostridiales* was the most abundant taxonomic group, followed by *Lactobacillales* (light blue). *Pseudomonadales* were among the least abundant taxonomic group in the uninfected controls (Fig. 4D). This was also observed when we analyzed the microbiome abundance of each individual animal in both infected and uninfected groups (Fig. S7). These results demonstrate that IAV infection induces a dynamic modulation of the microbiome structure in the URT of ferrets, which correlated with viral replication and pathogenesis. However, our data also suggests that the basal levels could be reestablished upon viral clearance, as observed in some human samples.

IAV infection differentiates the ferret URT microbiome structure into defined ecostates

Since the timing of infection was controlled in the ferret experiment, we hypothesized that upon infection the microbiome structure would be ordered into more defined ecostates for the infected

and uninfected animals. Hence, we run the iDMM model over 1000 iterations, which collapsed the data into two ecostates. The mean of the likelihood ratio at each iteration converged 70 iterations into the analysis, splitting into two ecostates until the last iteration. Of interest, one of the two ecostates was comprised of all the uninfected data points (or the "healthy" ecostate) while the other contained most of the influenza infected data points (the "unhealthy" ecostate, Table 2). There were notable exceptions; despite the perturbation caused by the infection, all Day 14 samples in the infected cohort moved from the "unhealthy" ecostate to the "healthy" ecostate, which is also shown in the ordination plot (Fig. 3). The healthy ecostate also contained a few of the earlier data points (Day 0 and Day 1) of the influenza-infected cohort, indicating a temporal lag in changes to the ferret microbiome at those time points when the IAV titer was submaximal (Fig. 4B).

The iDMM analysis for ferrets predicted the diagnostic OTU for the "unhealthy" ecostate to be Otu000004 that belonged to the *Pseudomonadales* order, with a posterior predictive probability of 0.11 (Table 3), followed by Otu000003 with the next highest predictive probability of 0.08, belonging more specifically to the *Pseudomonas* genus (Fig. S6). This is consistent with the qualitative taxonomic profiling (Fig. 4). For the "healthy" ecostate, Otu000001, which belongs to the *Clostridia* family, was the diagnostic OTU with a posterior predictive probability of 0.19 (Table 3). The posterior probabilities for each taxon were calculated within each sample by observing the fraction of simulated samples with more counts than the observed value. The probabilities associated with the diagnostic OTUs can be thought in terms of being relative to all taxa present. Similar to the human data, the diagnostic OTUs for both ecostates are among the ten most abundant OTUs for the data (Fig. S6). Remarkably, this was also confirmed when the microbiome for all ferrets from both infected and uninfected groups was analyzed individually

(Fig. S7), which indicates that *Pseudomonadales* are not only predictive of the unhealthy ecostate but also undergo the greatest temporal dynamic change during IAV infection. This was confirmed when alpha diversity analyses were conducted, which showed a drastic decrease in diversity by day 7 (Fig. S8). The results from the random forest analysis aligned well with the iDMM diagnostic OTU prediction in that Otu000004 (*Pseudomonadales*) was the most predictive attribute for the samples from IAV-infected ferrets, followed by Otu000028 (*Enterobacteriaceae*) and Otu000017 (*Bacillales*), with a maximum accuracy of 96% (Table S6). Altogether, these data indicates that IAV infection results in a nasal bloom of multiple *Pseudomonadales* in the ferrets, displacing the *Clostridia* associated with the "healthy" and stable ecostate.

Discussion

This longitudinal study describes taxonomic microbiome population dynamics in the upper respiratory tract of humans and ferrets during IAV infection. Given the unequivocal association between viral and bacterial co-infection and influenza disease severity, there is a pressing need to better understand how perturbation of the host microbiome correlates with viral infections that facilitate opportunistic co-infections. The nature of the 16S sequencing approach taken, that is a loci-based population survey, means that we can address taxonomy-centric ecological principles of disturbance and resilience (*27*, *28*) in the URT microbiome. Our results strongly suggest that the core URT microbiome is perturbed by IAV infection via direct and uncharacterized indirect processes, which may in turn might facilitate co-infections with bacterial pathogens causing increased hospitalizations and morbidity associated with IAV infection. Additionally, the results provide a clear approach for the design of future studies explicitly examining the mechanistic links between IAV and bacterial co-infection, along with the development of therapeutic treatments aimed at the microbiome as a community.

Without disturbance or perturbation, the URT microbiome was stable in both uninfected humans and ferrets. IAV does not directly infect any microbiome constituents, yet infection disturbs the healthy-state microbiome in both hosts in a statistically robust manner. The microbiomes of infected (unhealthy) individuals or animals were quite different from each other (Fig. 4, 2 and Fig. S2, S3, S5 and S6). However, in both hosts, unhealthy microbiomes were divergent from the healthy microbiomes and numerous community assemblies were possible in the unhealthy state. This is a clear demonstration of the Anna Karenina principle (*29*), restated as “all healthy microbiomes are the same, while unhealthy microbiomes are unique.” This high diversity of unhealthy microbiomes during early stages of acute infection is consistent with earlier studies

(*8*), but here we demonstrate specifically that it can occur as a consequence of an indirect disturbance such as IAV infection. We propose that the disturbance of the healthy URT microbiome creates transient ecological niches for opportunistic bacterial pathogens. How viral infection induces a disturbance in the microbiome requires further assessment. Nevertheless, the host antiviral responses such as the induction of interferon during IAV infection, could contribute to the perturbation of the microbiome in a dynamic manner, though this requires host and microbiome metatranscriptomics or metaproteomics measurements in controlled experiments focused at the onset of infection. Nevertheless, maximum disturbance correlated with maximum viral loads and weight loss in the ferret model, which suggests a close relationship between active infection, disease and disturbance of the microbiome, with kinetics that are similar to the antiviral response induced during IAV infection (*30*).

The sole statistical exception to the high community diversity of infected microbiomes was the increased relative abundance of *Pseudomonadales*, regardless of age, sex, antibiotic treatment, or even host organism. Oddly enough in humans, no significant influence of the host type (age and sex) or behavior (antibiotic usage) was observed on the temporal nature of the microbiome elasticity, and more statistical power would be needed to draw any further robust associations from the data. Yet, the "bloom" of *Pseudomonadales* is consistent with previous reports in H1N1-infected patients (*9, 15, 31, 32*). In our study, *Pseudomonadales* are present in relatively low proportions in the healthy microbiome of these host organisms. Therefore, their "bloom" might be due to a more hostile environment for the other taxa or perhaps a more hospitable environment for the *Pseudomonadales*, making this an excellent candidate for future strain isolation, genome sequencing, and transcriptional profiling. The increased abundance of *Pseudomonadales* and the decreased relative abundance of *Clostridiales* and *Actinobacteria* in

the infected cohorts suggest a potential use for probiotic treatments capable of modulating the microbiome back into the healthy ecostate (*33*). Such a treatment would be homologous to those proposed for perturbing or restoring the gut microbiome (*34*). Understanding how and why *Pseudomonadales* succeed after disturbance will provide valuable information for conducting future microbiome centric URT studies in a controlled setting. It should be noted that the blooming *Pseudomonads* are not *P. aeruginosa*, instead a variety of other related species within the genera, and understanding their functional potential and role requires shotgun metagenomics analyses for more detailed phylogenetic and functional profiling.

In addition, in humans secondary *Pseudomonas* infections have been extensively described before, and *Pseudomonas* infections have been specifically linked to nosocomial infections as a result respiratory support treatments in hospital settings (*35-39*). It is currently unknown whether infection with other respiratory viruses can also induce the modulation of the URT microbiome, however; since severe viral infections often require respiratory support, including intubation, it is likely that co-infection with pathogens such as the *Pseudomonadales* could actually be favored due to previous perturbations of the microbiome. Hence, additional associative studies to elucidate factors that modulate the temporal change of the microbiome structure could also aid in understanding the factors that promote or support secondary bacterial colonization during severe respiratory viral infections.

In the ferret model, there is a clear demonstration of ecological resilience in the URT microbiome; namely a return to the original community after disturbance, a phenomenon also observed, albeit less clearly, in the human samples, which had an unknown and likely more diverse ecostate prior to infection. Similar observations have been reported in the human gut microbiome after the massive disturbance associated with antibiotic treatment (*27*), though our

findings expands it to the URT and the indirect effects of the IAV infection. The controlled experiments with ferrets resulted in near complete recovery. Human URT microbiomes do not unequivocally show a return to the health state, but in several patients, the microbiome returned to the healthy ecostate. Although it is tempting to suggest that the ferret microbiome might have greater elasticity (i.e. less time required for demonstration of resilience), there are multiple potential reasons for the discrepancy between ferrets and humans. Considering metabolic rate relative to organism size, the ferret may recover at a more rapid rate simply due to a higher metabolism. More pertinently, the human cohort has an undetermined infection date, were infected by different viral strains (and viral variants as determined by whole IAV genome sequences) and had a selection bias towards phenotypically responsive patients (e.g. symptomatic hospitalized patients), where zero time (Day 0) was the first hospital visit. Beyond the potential differences in absolute temporal trends in microbiome resilience and elasticity, the human and ferret microbiomes share similar trends at the ecosystem and individual taxon level that warrant further experimentation. The results here provide an experimental baseline for examining both predictive and therapeutic intervention focused experiments in the ferret model system. For example, the presented hypothesis that IAV driven microbiome disturbance increases the propensity for bacterial pathogen co-infection can be robustly tested by bi-partite exposures to viral, and then bacterial pathogens. The effects of lifestyle (diet, smoking, exercise) and abiotic influences (humidity, temperature) on the microbiome and its resilience should also be examined, particularly with regards to temporal dynamics of microbiome disturbance and recovery. Potential therapeutic approaches involve thwarting the associated threat of opportunistic bacterial pathogens or interventions focused on the bloom of *Pseudomonas*, where probiotic treatments could be explored to maintain the homeostasis as seen in the healthy

individuals. Our results are especially relevant in the context of secondary bacterial infections following primary infection with IAV (*40*). Multiple studies, including this one, have now shown that a subset of the taxa that are most frequently associated with secondary infections have increased relative abundance during IAV infection. It is possible that such outcomes could be reduced by modulating the host immune response during IAV infection (*17*). Reducing the high morbidity and mortality rates associated with such secondary infections would improve quality of life and longevity while simultaneously reducing healthcare costs (*35*, *41*, *42*).

Materials and Methods

Human sample collection and study design

Patient clinical–epidemiological data, along with nasopharyngeal swabs were collected after informed written consent was obtained under protocol 11-116, reviewed and approved by the Scientific Ethics Committee of the School of Medicine at Pontificia Universidad Catolica de Chile (PUC) before the start of sample collection. Between July 2011 and November 2012, a total of 146 nasopharyngeal swabs samples were collected from 30 hospitalized patients in Santiago, Chile, diagnosed with influenza-like illness (ILI). Of the 30 patients in the study, 28 were confirmed and subtyped as H1N1pdm09 or H3N2 Influenza through RT-PCR by Clinical Virology Laboratory at PUC. The remaining 2 patients could not be confirmed as influenza positive by qRT-PCR, RT-PCR and/or the hemagglutination inhibition (HI) assay, but still displayed the perturbation in their microbiome so they were included in the analyses. Between one and six samples from the acute phase of infection were taken from each patient, together with a sample up to 22 days post diagnosis (convalescence phase or healthy baseline) from most of individuals. Control samples from 22 healthy individuals, confirmed as negative against

influenza A virus and 13 other common respiratory viruses, were taken with the same criteria in March to June of 2014. Epidemiological history, signs and symptoms, other diagnostics and treatments of each patient were also collected during hospitalization as detailed in Table S3. Furthermore, 96.4% of patients received oseltamivir antiviral treatment and 89.3% received antibiotics originating from the families of the fluoroquinolones (levofloxacine, morifloxacine or ciprofloxacine), 3rd generation cephalosporins (ceftriaxone or cefepime), carbapenems (meropenem or imipenem), metrodinazole, cotrimoxazole or vancomycin. These treatments where supplied in a combination of 5 (4% of patients), 4 (8%), 3 (12%), 2 (40%) or one (36%) antibiotics in a complete treatment (at least seven days) or less. Severe infection criteria were established in accordance with the hospitalization due to influenza and/or derivation to Critical Care Unit (which involves oxygen support or mechanical ventilation and/or vasoactive drug administration) after symptoms onset. The microbiome data analyzed were obtained from the nasopharyngeal swabs of 33 infected subjects (14 male and 19 female), ages ranging from one year to 76 years, for a total of 146 samples. The naming convention of influenza A viruses detected from patients are as follows: A/Santiago/p*x*d*y*/2011 or A/Santiago/p*x*d*y*/2012 (p=patient and d=day). The negative controls analyzed in the study were nasopharyngeal swabs taken from 22 healthy patients (10 males and 12 females), most taken at all 6 time points (1, 2, 3, 5, 8 and 28 dpi), for a total of 127 samples, which were negative for influenza and other respiratory infections.

Ferret infection and sample collection

The animal experiments described here were performed under protocols approved by the Icahn School of Medicine at Mount Sinai Institutional Animal Care and Use Committee, adhering

strictly to the NIH Guide for the Care and Use of Laboratory Animals. Six months old female ferrets (*Mustela putorious furo*) were confirmed to be seronegative against circulating H1N1, H3N2 and B influenza viruses before they purchased from Triple F Farms. Throughout the experiment the animals were housed individually in PlasLabs poultry incubators with access to food and water *ad libitum*. All infections and nasal wash samples were done on ferrets anesthetized with ketamine (25 mg/kg) and xylazine (2mg/kg) intramuscularly. A detailed time point study was conducted in ferrets infected with $1x10^6$ plaque forming units diluted in a final volume of 5.0 ml of sterile PBS per animal of the A/Netherlands/602/2009 H1N1 pandemic strain through intranasal inoculation. Control animals were mock infected only with 0.5 ml of sterile PBS. Then nasal wash samples were taken from the 7 uninfected and 7 infected animals. To study the effect of IAV infection on the URT microbiome, samples were taken at 6 different timepoints: on day 0 (1 hr post inoculation) and then on days 1, 3, 5, 7 and 14 post infection (dpi). Body weights were obtained for 14 consecutive days, and viral titers were determined by plaque assay in MDCK cells as previously described (*43*) for the first 7 dpi.

Sample processing and sequence analyses

All bacterial genomic DNA (gDNA) extractions were performed using the Qiagen All Prep kit and were subjected to 16S amplification using the HMP 16S sequencing protocol and the amplicons were sequenced using the Roche 454 Titanium pipeline (*44*). Appropriate positive and negative controls from amplification were also included. The V1-V3 hypervariable regions were amplified for 16S profiling (forward primer: 27F 5'- AGAGTTTGATCCTGGCTCAG-3' and reverse primer: 534R 5'- ATTACCGCGGCTGCTGG-3') of the 16S ribosomal RNA gene.

Data Analysis

Reads were de-multiplexed according to barcodes followed by trimming of both barcodes and adapter sequences. Following the initial processing of the sequence data, sequences were combined, dereplicated and aligned in mothur (version 1.36.1 (*45*)) using the SILVA template (*46*) (SSURef_NR99_123) and the sequences were organized into clusters of representative sequences based on taxonomy called Operational Taxonomic Units (OTU) using the UPARSE pipeline (*47*). In the ferrets, all except two libraries generated more than 3000 reads per sample. A total of 649,440 sequences were subsequently clustered into 259 OTUs with a sequence similarity threshold of 97% (*45*), a length threshold of 250 bp and an expected error threshold of 0.15. For human samples, the distribution of reads per sample was much more uneven. A total of 2,342,992 sequences were sorted into 707 OTUs, using the same thresholds as above and the same downstream filtering of the OTUs and samples was performed in a similar manner. Initial filtering of the samples ensured discarding samples containing less than 5 sequences. Libraries were normalized using metagenomeSeq's cumulative sum scaling method (*48*) to account for library size acting as a confounding factor for the beta diversity analysis. In addition to discarding singletons, OTUs that were observed fewer than 5 times in the count data were also filtered out to avoid the inflation of any contaminants that might skew the diversity estimates.

Informatics

Beta diversity metrics were calculated across all samples using the Bray-Curtis dissimilarity index and overall trends in the community composition for ferrets and humans on the basis of

presence or absence of the flu infection were explored using Principal Coordinates Analysis (PCoA) in QIIME (*49*) (version 1.9.1) and then visualized in Emperor (*50*) (version 0.9.51).

Taxonomic classification of the samples was done by classifying the representative sequences from the OTUs using mothur and the SILVA database, with a confidence threshold of 97%. The relative abundances for the taxonomic profiles for each subject was calculated in QIIME using summarize_taxa.py. The visualization of the top ten most prevalent taxa for each of the organisms was done in R (version 3.2.2) using dplyr and reshape2 to manipulate the data and ggplot2 for generating the plots. Following the qualitative analysis of the data, we employed an infinite dimensional generalization of the multinomial Dirichlet mixture model (*21*) which tries to model the original set of communities from the input data with additional posterior predictive probabilities (PPD) for statistical cut offs. The model was executed over 1000 iterations for the ferret data and 2000 iterations for the human data since this parameter should increase with the number of samples present in the dataset. Scripts located at https://github.com/jacobian1980/ecostates were improved by introducing a seed in the beginning of the algorithm to improve the reproducibility of the model and optimized the community number based on the PPDs which compare empirically observed data with the data that would be expected if the DMM were the correct underlying model (*51, 52*). All downstream analyses with the communities, including exploration of community membership, were performed in R. Additionally, a diagnostic OTU was computed for each ecostate, or sampled community, which is the OTU with the highest posterior predictive probability in the ecostate and therefore drives the clustering. The quantitative portion of the analysis was supplemented by performing random forest classification on the data to confirm the diagnostic results using Scikit-Learn (version

0.18.1) in Python (version 3.5.2) from Continuum Analytics Anaconda Suite. The training dataset included: a *(n x m)*-dimensional attribute matrix consisting of the relative abundance values for the OTUs and the samples, where n and m refer to the number of samples and the number of OTUs respectively, and a (*n)*-dimensional vector relating each observation to the 2 experimental states (positive and negative for the virus). The average of the feature importance vectors from 20000 models that could accurately predict all 5 left-out samples (~85% accuracy) was computed to obtain a weight for each OTU's predictive capacity to classify the experimental state of each sample. The hyperparameters for the random forest model were 618 decision trees per forest, gini index as impurity criterion and the square root of the number of features (OTUs in this case) to use for each split in the decision tree.

Data Availability: Raw amplicon sequence reads for this study have been deposited to Sequence Read Archive (SRA) under accession number: SRP009696 [BioProject accession number: PRJNA76689] for the ferrets and accession numbers: SRP092459 [BioProject accession number: PRJNA240559] and SRP128464 [PRJNA240562] for the infected and uninfected human subjects respectively.

References and Notes:

1. A. D. Iuliano *et al.*, Estimates of global seasonal influenza-associated respiratory mortality: a modelling study. *Lancet*, (2017).
2. N. P. Johnson, J. Mueller, Updating the accounts: global mortality of the 1918-1920 "Spanish" influenza pandemic. *Bull Hist Med* **76**, 105-115 (2002).
3. J. F. Brundage, Interactions between influenza and bacterial respiratory pathogens: implications for pandemic preparedness. *Lancet Infect Dis* **6**, 303-312 (2006).
4. J. F. Brundage, G. D. Shanks, Deaths from bacterial pneumonia during 1918-19 influenza pandemic. *Emerg Infect Dis* **14**, 1193-1199 (2008).

5. D. M. Morens, J. K. Taubenberger, A. S. Fauci, Predominant role of bacterial pneumonia as a cause of death in pandemic influenza: implications for pandemic influenza preparedness. *J Infect Dis* **198**, 962-970 (2008).
6. C. C. Blyth *et al.*, The impact of bacterial and viral co-infection in severe influenza. *Influenza Other Respir Viruses* **7**, 168-176 (2013).
7. N. S. Shah *et al.*, Bacterial and viral co-infections complicating severe influenza: Incidence and impact among 507 U.S. patients, 2013-14. *J Clin Virol* **80**, 12-19 (2016).
8. E. S. Charlson *et al.*, Topographical continuity of bacterial populations in the healthy human respiratory tract. *Am J Respir Crit Care Med* **184**, 957-963 (2011).
9. Y. Tarabichi *et al.*, The administration of intranasal live attenuated influenza vaccine induces changes in the nasal microbiota and nasal epithelium gene expression profiles. *Microbiome* **3**, 74 (2015).
10. S. Langevin *et al.*, Early nasopharyngeal microbial signature associated with severe influenza in children: a retrospective pilot study. *J Gen Virol*, (2017).
11. Z. Gao, Y. Kang, J. Yu, L. Ren, Human pharyngeal microbiome may play a protective role in respiratory tract infections. *Genomics Proteomics Bioinformatics* **12**, 144-150 (2014).
12. Y. J. Huang, S. V. Lynch, The emerging relationship between the airway microbiota and chronic respiratory disease: clinical implications. *Expert Rev Respir Med* **5**, 809-821 (2011).
13. P. J. Planet *et al.*, Lambda Interferon Restructures the Nasal Microbiome and Increases Susceptibility to Staphylococcus aureus Superinfection. *MBio* **7**, e01939-01915 (2016).
14. F. J. Whelan *et al.*, The loss of topography in the microbial communities of the upper respiratory tract in the elderly. *Ann Am Thorac Soc* **11**, 513-521 (2014).
15. B. Chaban *et al.*, Characterization of the upper respiratory tract microbiomes of patients with pandemic H1N1 influenza. *PLoS One* **8**, e69559 (2013).
16. T. Ichinohe *et al.*, Microbiota regulates immune defense against respiratory tract influenza A virus infection. *Proc Natl Acad Sci U S A* **108**, 5354-5359 (2011).
17. J. Wang *et al.*, Bacterial colonization dampens influenza-mediated acute lung injury via induction of M2 alveolar macrophages. *Nat Commun* **4**, 2106 (2013).
18. S. Wu *et al.*, Microbiota regulates the TLR7 signaling pathway against respiratory tract influenza A virus infection. *Curr Microbiol* **67**, 414-422 (2013).
19. J. A. Belser, A. M. Eckert, T. M. Tumpey, T. R. Maines, Complexities in Ferret Influenza Virus Pathogenesis and Transmission Models. *Microbiol Mol Biol Rev* **80**, 733-744 (2016).
20. J. A. Belser, J. M. Katz, T. M. Tumpey, The ferret as a model organism to study influenza A virus infection. *Disease Models & Mechanisms* **4**, 575-579 (2011).
21. J. D. O'Brien, N. Record, P. Countway, The power and pitfalls of Dirichlet-multinomial mixture models for ecological count data. *bioRxiv*, (2016).
22. I. Holmes, K. Harris, C. Quince, Dirichlet Multinomial Mixtures: Generative Models for Microbial Metagenomics. *PLOS ONE* **7**, e30126 (2012).
23. M. Menuet *et al.*, First isolation of two colistin-resistant emerging pathogens, Brevundimonas diminuta and Ochrobactrum anthropi, in a woman with cystic fibrosis: a case report. *J Med Case Rep* **2**, 373 (2008).
24. Y. J. Huang *et al.*, A persistent and diverse airway microbiota present during chronic obstructive pulmonary disease exacerbations. *OMICS* **14**, 9-59 (2010).

25. R. P. Dickson, J. R. Erb-Downward, G. B. Huffnagle, Homeostasis and its disruption in the lung microbiome. *Am J Physiol Lung Cell Mol Physiol* **309**, L1047-1055 (2015).
26. A. A. Heirali *et al.*, The effects of inhaled aztreonam on the cystic fibrosis lung microbiome. *Microbiome* **5**, 51 (2017).
27. D. A. Relman, The human microbiome: ecosystem resilience and health. *Nutrition reviews* **70**, S2-S9 (2012).
28. B. Walker, C. S. Holling, S. R. Carpenter, A. Kinzig, Resilience, adaptability, and transformability in social-ecological systems. *Ecology and Society* **9**, 5 (2004).
29. J. R. Zaneveld, R. McMinds, R. Vega Thurber, Stress and stability: applying the Anna Karenina principle to animal microbiomes. *Nature Microbiology* **2**, 17121 (2017).
30. M. J. Killip, E. Fodor, R. E. Randall, Influenza virus activation of the interferon system. *Virus Res* **209**, 11-22 (2015).
31. E. Y. Klein *et al.*, The frequency of influenza and bacterial coinfection: a systematic review and meta-analysis. *Influenza Other Respir Viruses* **10**, 394-403 (2016).
32. R. K. Leung *et al.*, Modulation of potential respiratory pathogens by pH1N1 viral infection. *Clin Microbiol Infect* **19**, 930-935 (2013).
33. H. W. Chen *et al.*, Nasal commensal Staphylococcus epidermidis counteracts influenza virus. *Sci Rep* **6**, 27870 (2016).
34. J. K. Spinler *et al.*, From prediction to function using evolutionary genomics: human-specific ecotypes of Lactobacillus reuteri have diverse probiotic functions. *Genome Biol Evol* **6**, 1772-1789 (2014).
35. D. E. Morris, D. W. Cleary, S. C. Clarke, Secondary Bacterial Infections Associated with Influenza Pandemics. *Front Microbiol* **8**, 1041 (2017).
36. A. Hotterbeekx *et al.*, The endotracheal tube microbiome associated with Pseudomonas aeruginosa or Staphylococcus epidermidis. *Sci Rep* **6**, 36507 (2016).
37. J. Rello, Bench-to-bedside review: Therapeutic options and issues in the management of ventilator-associated bacterial pneumonia. *Crit Care* **9**, 259-265 (2005).
38. Q. Lu *et al.*, Pseudomonas aeruginosa serotypes in nosocomial pneumonia: prevalence and clinical outcomes. *Crit Care* **18**, R17 (2014).
39. G. Hoffken, M. S. Niederman, Nosocomial pneumonia: the importance of a de-escalating strategy for antibiotic treatment of pneumonia in the ICU. *Chest* **122**, 2183-2196 (2002).
40. N. Sharma-Chawla *et al.*, Influenza A Virus Infection Predisposes Hosts to Secondary Infection with Different Streptococcus pneumoniae Serotypes with Similar Outcome but Serotype-Specific Manifestation. *Infect Immun* **84**, 3445-3457 (2016).
41. R. K. Gupta, R. George, J. S. Nguyen-Van-Tam, Bacterial pneumonia and pandemic influenza planning. *Emerg Infect Dis* **14**, 1187-1192 (2008).
42. J. C. Kash, J. K. Taubenberger, The role of viral, host, and secondary bacterial factors in influenza pathogenesis. *Am J Pathol* **185**, 1528-1536 (2015).
43. B. Manicassamy *et al.*, Protection of mice against lethal challenge with 2009 H1N1 influenza A virus by 1918-like and classical swine H1N1 based vaccines. *PLoS Pathog* **6**, e1000745 (2010).
44. M. Margulies *et al.*, Genome sequencing in microfabricated high-density picolitre reactors. *Nature* **437**, 376-380 (2005).
45. P. D. Schloss *et al.*, Introducing mothur: open-source, platform-independent, community-supported software for describing and comparing microbial communities. *Appl Environ Microbiol* **75**, 7537-7541 (2009).

46. C. Quast *et al.*, The SILVA ribosomal RNA gene database project: improved data processing and web-based tools. *Nucleic Acids Res* **41**, D590-596 (2013).
47. R. C. Edgar, UPARSE: highly accurate OTU sequences from microbial amplicon reads. *Nat Methods* **10**, 996-998 (2013).
48. J. N. Paulson, O. C. Stine, H. C. Bravo, M. Pop, Differential abundance analysis for microbial marker-gene surveys. *Nature Methods* **10**, 1200 (2013).
49. J. G. Caporaso *et al.*, QIIME allows analysis of high-throughput community sequencing data. *Nat Methods* **7**, 335-336 (2010).
50. Y. Vazquez-Baeza, M. Pirrung, A. Gonzalez, R. Knight, EMPeror: a tool for visualizing high-throughput microbial community data. *Gigascience* **2**, 16 (2013).
51. A. Gelman, X.-L. Meng, H. Stern, POSTERIOR PREDICTIVE ASSESSMENT OF MODEL FITNESS VIA REALIZED DISCREPANCIES. *Statistica Sinica* **6**, 733-760 (1996).
52. X.-L. Meng, Multiple-Imputation Inferences with Uncongenial Sources of Input. *Statist. Sci*. **9**, 538-558 (1994).

Acknowledgements:

The authors would like to thank research nurse Claudia Marco and the following clinical fellows and pediatricians that contributed to the recruitment of patients and the collection of samples used in this study: Marta Aravena, Catalina Gutierrez, Tania Lopez, Regina Perez and Cecilia Vizcaya from the Department of Pediatric Infectious Diseases and Immunology, Facultad de Medicina, Pontificia Universidad Católica de Chile, Santiago, Chile. Funding: This project has been partly funded with federal funds from the National Institute of Allergy and Infectious Diseases, National Institutes of Health, Department of Health and Human Services under Contract Number HHNS272200900007C/ HHSN266200700010C and Grant Number U19AI110819, grants from the Comisión Nacional de Investigación Científica y Tecnológica (FONDECYT 1121172 and 1161791 to R.A.M.; and PIA ACT 1408 to R.A.M. and M.F.), and the Chilean Ministry of Economy, Development and Tourism (P09/016-F to R.A.M.). This study was also partially supported by CRIP (Center for Research in Influenza Pathogenesis), an NIAID funded Center of Excellence for Influenza Research and Surveillance (CEIRS, contract # HHSN272201400008C) and by NIAID grant U19AI135972 (to A.G.-S. and R.A.M.).

Author Contributions: D.K. and R.R. analyzed data, prepared illustrations, and wrote the manuscript. M.F. designed human cohort study, recruited patients, collected clinical metadata and wrote parts of the paper. G.S.T., B.E.P. carried out data analysis and wrote parts of the paper. A.B. carried out data analysis, prepared illustrations, and wrote parts of the paper. D.W. and B.M. obtained funding, designed and supervised experiments and analyzed data. S.D. supervised experiments and analyzed data. I.B. recruited patients and collected clinical metadata. R.A.H. performed sequencing experiments and metadata compilation. M.S., I.M., R.A.A. performed ferret experiments. I.S. performed data processing and analysis. K.E.N. Obtained

funding, supervised this study and wrote parts of the paper. A.G.S. conceived and supervised this study and wrote the manuscript. C.L.D. supervised this study, designed informatics analyses, analyzed data, prepared illustrations, and wrote the manuscript. R.A.M. obtained funding, conceived and supervised this study, designed and performed experiments, analyzed data, prepared illustrations, and wrote the manuscript.

Competing Interests: The authors declare no competing interests.

Figures

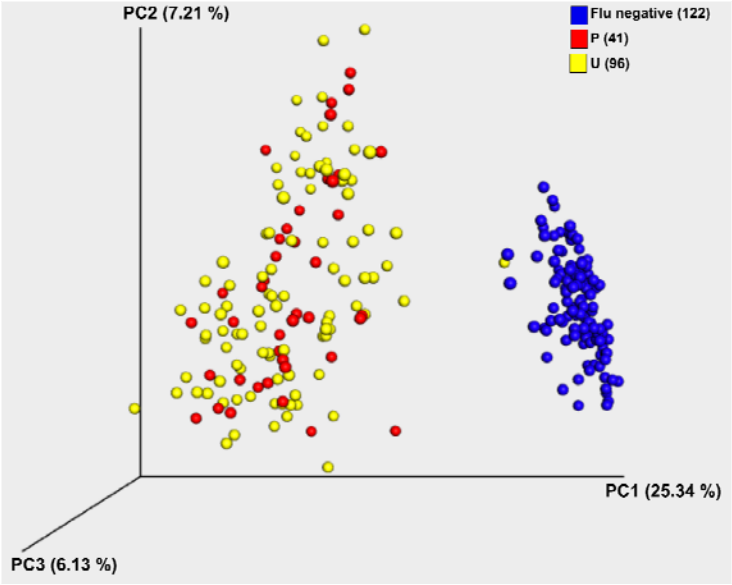

Figure 1. Diversity of the URT microbiome of human patients infected with influenza A virus (IAV). Beta diversity analysis for longitudinal nasopharyngeal swab samples obtained from heathy and IAV infected individuals. Principal coordinates analysis (PCoA) of Bray Curtis distances was done for samples from humans, labeled as influenza positive in red (P, indicating data points with positive IAV qRT-PCR detection), influenza unknown in yellow (U, indicates time points from positive individuals that were below the qRT-PCR detection limits at different time points after the onset of symptoms) and uninfected samples in blue (Flu negative). The total variability explained by all three principal coordinates (PCs) is shown on the axes.

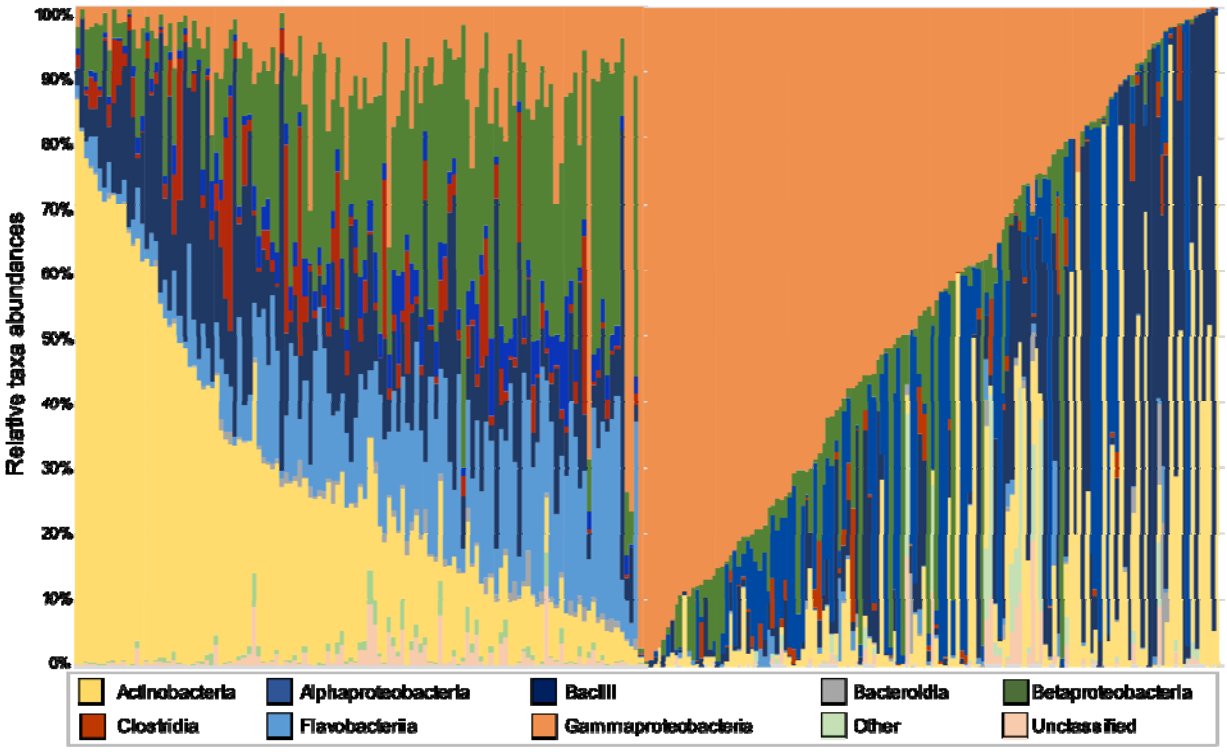

Figure 2. Comprehensive taxonomic breakdown for IAV-free (left) and IAV-infected (right) human subjects. The plot summarizes the relative taxonomic abundances at the class level for taxonomic groups that are present in greater than 5% of the samples (see legend below). Gammaproteobacteria (*Pseudomonas*, orange) bloom is prevalent among the infected patients (right), whereas Actinobacteria is the most abundant among healthy patients.

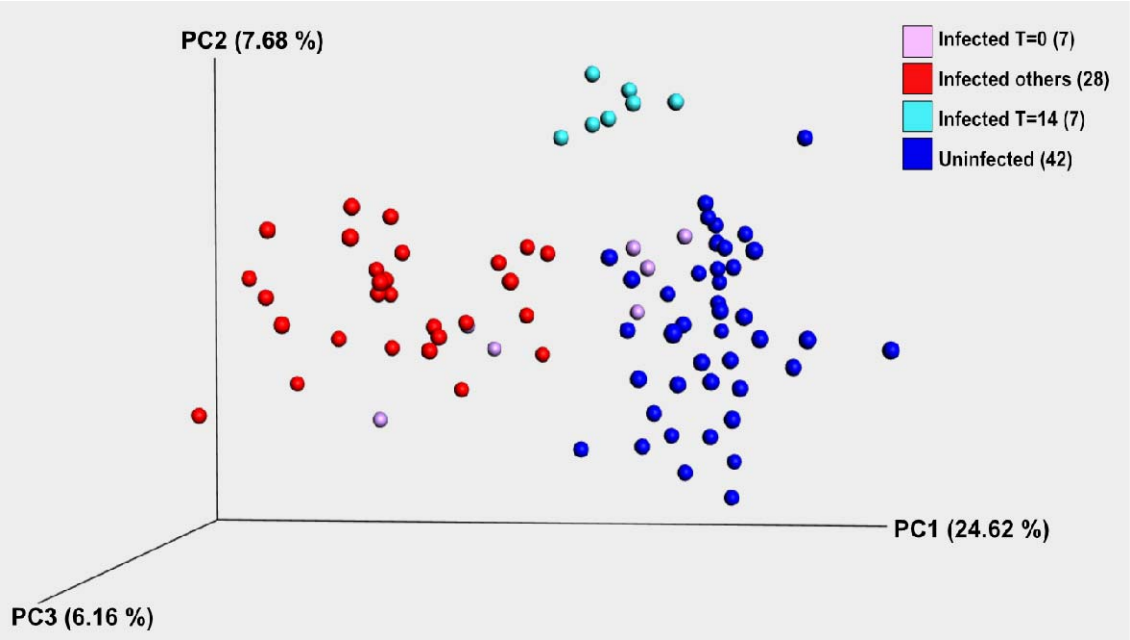

Fig. 3: Diversity of the URT microbiome in ferrets during IAV infection. Beta diversity analysis for longitudinal URT samples taken after experimental infection with the A/Netherlands/602/09 H1N1 strain (Infected) or in control animals. Principal coordinates analysis (PCoA) of Bray Curtis distances was performed for all samples. Data points for uninfected ferrets are in blue, the T=0 for the infected ferrets in lavender, the T=14 for infected ferrets in cyan, and all other infected time points are in red. The total variability explained by all three principal coordinates (PCs) is shown on the axes. Each group of ferret was composed of 7

animals.

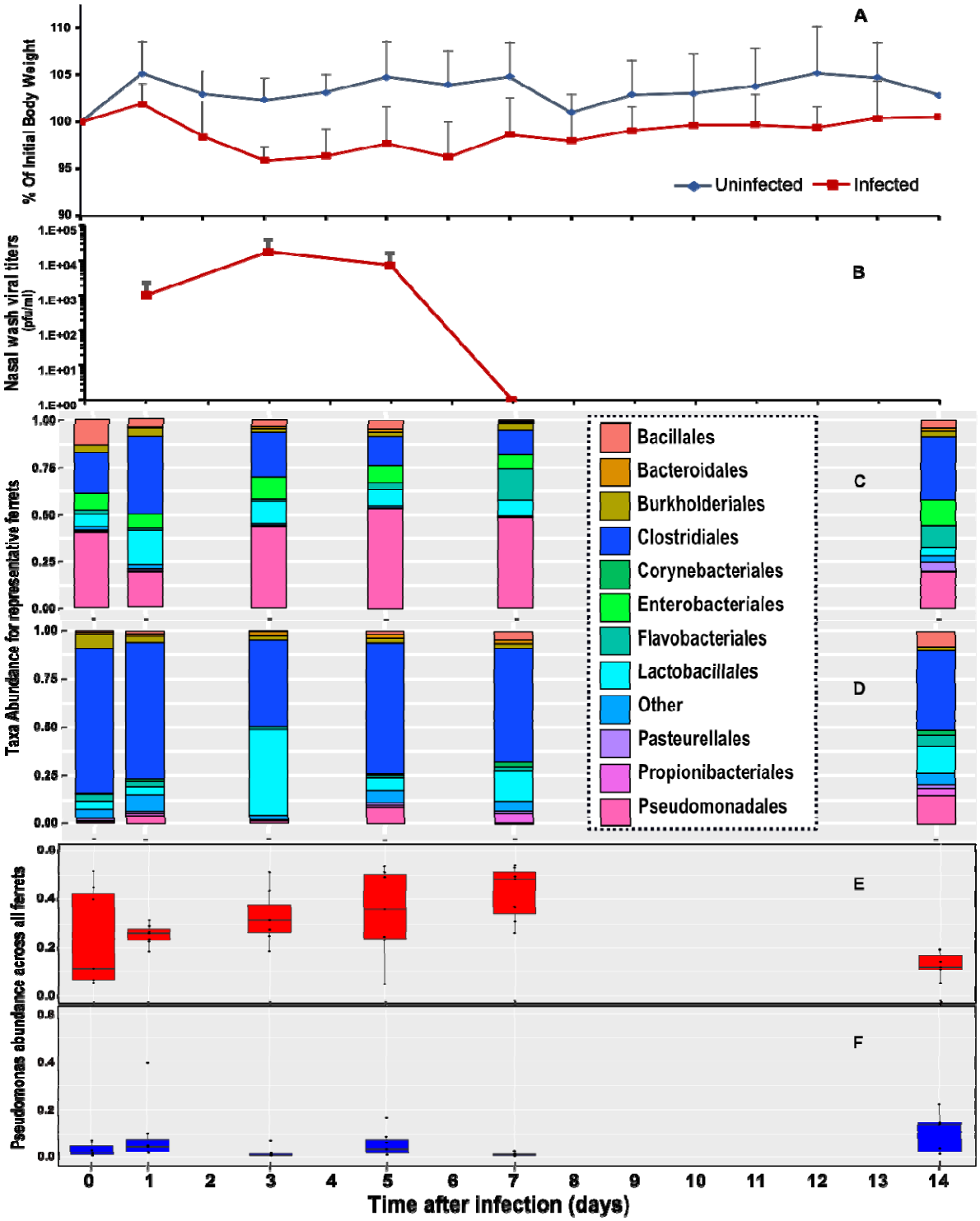

Fig. 4. Qualitative and quantitative representation of the temporal trajectory of the ferret microbiome. (A) Percent body weights of groups of 7 ferrets mock inoculated (uninfected) or

intranasally infected with $1X10^6$ pfu of influenza A/Neth/602/09 virus. Body weights were determined daily for 14 days, and are represented as the average percent body weight compared to the initial weight of each animal on the day of inoculation and error bars are the standard deviation for each time point. (B) Viral titers of nasal washes of ferrets infected with $1X10^6$ pfu of A/Neth/602/09 virus. Nasal washes were obtained on days 1, 3, 5 and 7 post infection and are represented as the average viral titer of 7 infected animals. Error bars indicate the standard deviation for each time point. (C-D) Comprehensive taxonomic breakdown of an influenza infected (C) and uninfected ferret (D), at different timepoints. Taxa abundance values for top ten most prevalent taxa at the order level for different timepoints (0 to14 dpi). Only taxa labels with a confidence score of >= 90% were retained in the analysis. The remaining taxa are pooled into an additional taxon labeled "Other". (E-F) Average and standard deviation of the relative *Pseudomonas* abundance across all infected (E) and uninfected (F) ferrets (n=7 for each).

TABLES

Table 1. Summary statistics for amplicon-based sequencing of the V1-V3 region of the 16S rRNA gene.

	Humans	**Ferrets**
Total no. of samples[a]	273	86
Influenza negative subjects	22	7
Influenza positive subjects	33	7
Total no. of reads	2 342 992	649 440
Total no. of OTUs	707	259
No. of reads mapped to OTUs	2 151 233 (91.8%)	514 099 (79.2%)

a. All ferret and human samples were extracted from nasal washes and nasopharyngeal swabs, respectively, at several time points post infection.

Table 2. Diagnostic microbes for each ecostate from the 2000th iteration of the iDMM model for the infected and uninfected humans. Number of iterations depends on the number of samples (273) present in the data.

Ecostate	Final distribution[a]	Original sample distribution[b]	Diagnostic OTU	Probability associated[c]	Taxonomy
1 + 2 + 3 (Infected)	114	146	Otu000003	0.361568	Bacteria;Proteobacteria; Gammaproteobacteria;Pseudomonadales; Pseudomonadaceae;Pseudomonas
	9		Otu000004	0.4989514	Bacteria;Actinobacteria; Actinobacteria;Corynebacteriales; Corynebacteriaceae; Corynebacterium_1
	20		Otu000002	0.01584407	Bacteria;Proteobacteria; Gammaproteobacteria; Pseudomonadales;unclassified
4 (Healthy)	130	127	Otu000008	0.07636954	Bacteria;Bacteroidetes; Flavobacteriia;Flavobacteriales; Flavobacteriaceae;Cloacibacterium

a. Distribution of samples within ecostates after running the iDMM model.

b. Distribution of samples before running the iDMM model.

c. Bayesian posterior predictive probabilities associated with the diagnostic microbe, which is the highest probability for that ecostate.

Table 3. Diagnostic microbes for each ecostate from the 1000th iteration of the iDMM model for the ferret samples. Number of iterations depends on the total number of samples (84) present in the data. All later time point ferrets (T14) return to the healthy ecostate (1).

Ecostate	Total samples	No. of samples[a] T14	[T7 + T5 + T3 + T1]	T0	Diagnostic OTU	Probability associated[b]	Taxonomy
1 (Healthy)	**58** (42)	**14** (7)	**33** (28)	**11** (7)	Otu000001	0.1865749	Bacteria;Firmicutes; Clostridia;Clostridiales; Peptostreptococcaceae; Romboutsia
2 (Infected)	**26** (42)	**0** (7)	**23** (28)	**3** (7)	Otu000004	0.1112045	Bacteria;Proteobacteria; Gammaproteobacteria; Pseudomonadales; Moraxellaceae; Acinetobacter

a. No. of samples at final iteration for each time point in bold (original starting values in parentheses).

b. Bayesian posterior predictive probabilities associated with the microbe, which is the highest probability for that ecostate.

Supplementary Materials:

Figure S1. Diversity distance analyses of the microbiome of infected and uninfected humans.

Figure S2. Relative abundance for the top ten bacterial families in the URT among infected and uninfected human subjects.

Figure S3. Comprehensive taxonomic breakdown for influenza-infected human subjects.

Figure S4. Comprehensive temporal taxonomic breakdown for 6 human subjects.

Figure S5. Diversity distance analyses of the microbiome of infected and uninfected ferrets.

Figure S6. Relative abundance for the top ten most prevalent bacterial families in the URT among infected and uninfected ferrets.

Figure S7. Comprehensive taxonomic breakdown for all 14 ferrets.

Table S1. Clinical-epidemiological characteristics of the hospitalized human patients diagnosed with Influenza A-like illness, and healthy controls.

Table S2. Two-sided Student's two sample t test results for human samples.

Table S3. Non-parametric multivariate analysis using Anosim and Adonis tests.

Table S4: Random forest analysis results for the human microbiomes.

Table S5. Two-sided Student's two sample t test results for ferrets.

Table S6. Random forest analysis results for the ferret microbiomes.

Supplemental information for

Microbiome disturbance and resilience dynamics of the upper respiratory tract in response to influenza A virus infection in humans and ferrets

Drishti Kaul[1,8], Raveen Rathnasinghe[2,8], Marcela Ferres[2], Gene S. Tan[1,3], Aldo Barrera[2,4], Brett E. Pickett[5], Barbara A. Methe[5], Suman Das[5], Isolda Budnik[2], Rebecca Halpin[5], David Wentworth[5b], Mirco Schmolke[6c], Ignacio Mena[6], Randy A. Albrecht[6], Indresh Singh[5], Karen E. Nelson[5], Adolfo Garcia-Sastre[6,7], Chris L. Dupont[1*], Rafael A. Medina[2,4,6*].

[1]J. Craig Venter Institute, 4120 Capricorn Lane, La Jolla, CA 92037, USA.

[2]Departmento de Enfermedades Infecciosas e Inmunología Pediátrica, Facultad de Medicina, Pontificia Universidad Católica de Chile, Santiago, Chile.

[3] Department of Infectious Diseases, University of California San Diego, La Jolla, CA 92037, USA

[4]Millennium Institute on Immunology and Immunotherapy, Santiago, Chile

[5]J. Craig Venter Institute, 9704 Medical Center Drive, Rockville, Maryland 20850, 14 USA.

[6]Department of Microbiology, Global Health and Emerging Pathogens Institute, Icahn School of Medicine at Mount Sinai, New York, NY 10029, USA.

[7]Department of Medicine, Icahn School of Medicine at Mount Sinai, New York, NY 10029, USA.

[8]These authors contributed equally to this work

[b] Present address: National Center for Immunization and Respiratory Diseases, Centers for Disease Control and Prevention, Atlanta, GA, USA.

[c] Present address: Department of Microbiology and Molecular Medicine, University of Geneva, Switzerland

*Corresponding author: E-mail: rmedinas@med.puc.cl , cdupont@jcvi.org

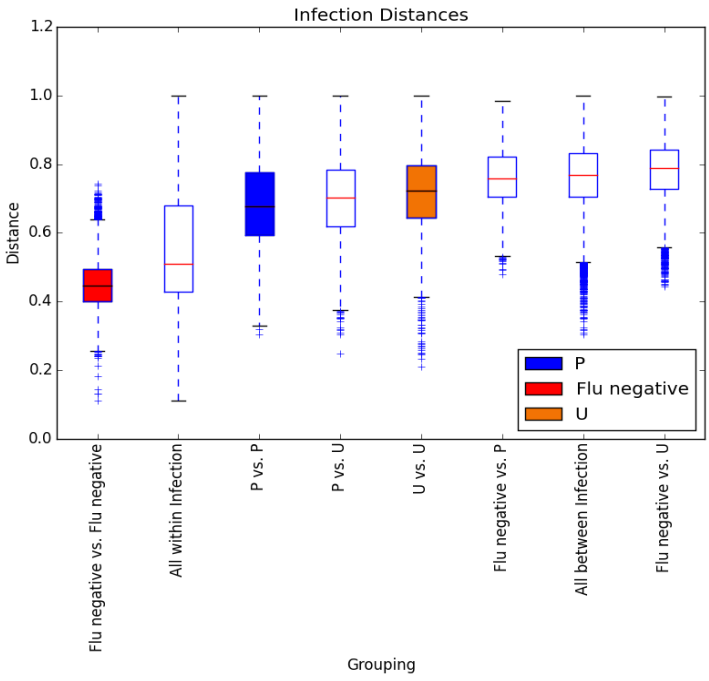

Figure S1. Diversity distance analyses of the microbiome of infected and uninfected humans. Box and whisker plots for beta diversity distances within and between influenza types for the human samples (P: Influenza positive, U: Influenza unknown, Flu negative). The boxplots represent the diversity between the different infection types. All the distances were calculated using the Bray-Curtis metric. Red line indicates median in each of the sample groupings and the error bars represent standard deviation.

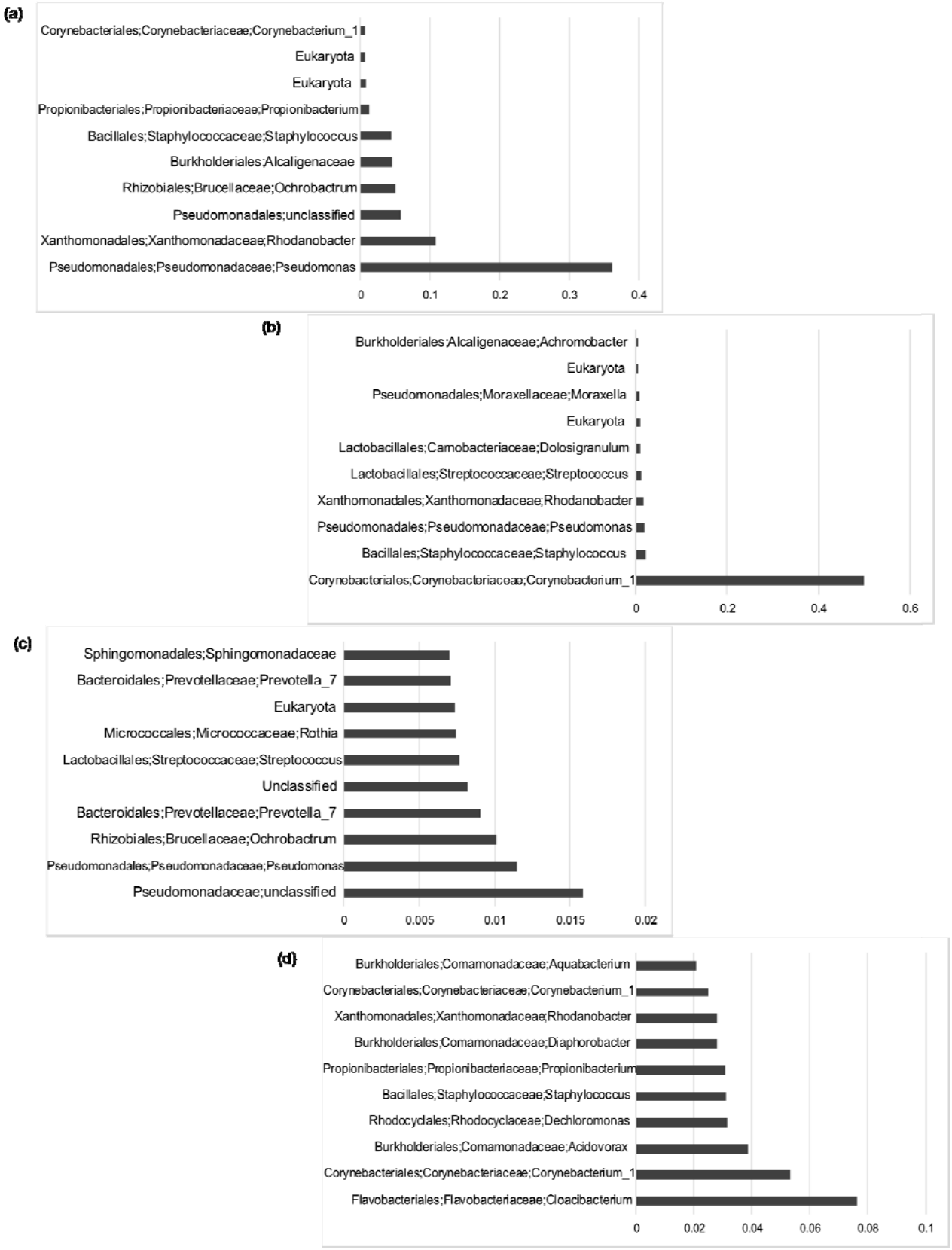
(a)
Corynebacteriales;Corynebacteriaceae;Corynebacterium_1
Eukaryota
Eukaryota
Propionibacteriales;Propionibacteriaceae;Propionibacterium
Bacillales;Staphylococcaceae;Staphylococcus
Burkholderiales;Alcaligenaceae
Rhizobiales;Brucellaceae;Ochrobactrum
Pseudomonadales;unclassified
Xanthomonadales;Xanthomonadaceae;Rhodanobacter
Pseudomonadales;Pseudomonadaceae;Pseudomonas
0
0.1
0.2
0.3
0.4
(b)
Burkholderiales;Alcaligenaceae;Achromobacter
Eukaryota
Pseudomonadales;Moraxellaceae;Moraxella
Eukaryota
Lactobacillales;Carnobacteriaceae;Dolosigranulum
Lactobacillales;Streptococcaceae;Streptococcus
Xanthomonadales;Xanthomonadaceae;Rhodanobacter
Pseudomonadales;Pseudomonadaceae;Pseudomonas
Bacillales;Staphylococcaceae;Staphylococcus
Corynebacteriales;Corynebacteriaceae;Corynebacterium_1
0
0.2
0.4
0.6
(c)
Sphingomonadales;Sphingomonadaceae
Bacteroidales;Prevotellaceae;Prevotella_7
Eukaryota
Micrococcales;Micrococcaceae;Rothia
Lactobacillales;Streptococcaceae;Streptococcus
Unclassified
Bacteroidales;Prevotellaceae;Prevotella_7
Rhizobiales;Brucellaceae;Ochrobactrum
Pseudomonadales;Pseudomonadaceae;Pseudomonas
Pseudomonadaceae;unclassified
0
0.005
0.01
0.015
0.02
(d)
Burkholderiales;Comamonadaceae;Aquabacterium
Corynebacteriales;Corynebacteriaceae;Corynebacterium_1
Xanthomonadales;Xanthomonadaceae;Rhodanobacter
Burkholderiales;Comamonadaceae;Diaphorobacter
Propionibacteriales;Propionibacteriaceae;Propionibacterium
Bacillales;Staphylococcaceae;Staphylococcus
Rhodocyclales;Rhodocyclaceae;Dechloromonas
Burkholderiales;Comamonadaceae;Acidovorax
Corynebacteriales;Corynebacteriaceae;Corynebacterium_1
Flavobacteriales;Flavobacteriaceae;Cloacibacterium
0
0.02
0.04
0.06
0.08
0.1

808

Figure S2. Relative abundance for the top ten bacterial families in the URT among infected and uninfected human subjects. The relative abundance values for the most prevalent bacterial families among the infected (a, b, and c) and uninfected (d) human samples based on the Bayesian posterior predictive probabilities from the Infinite Dirichlet Multinomial mixture Models run over 2000 iterations (top to bottom, (a)-(d)).

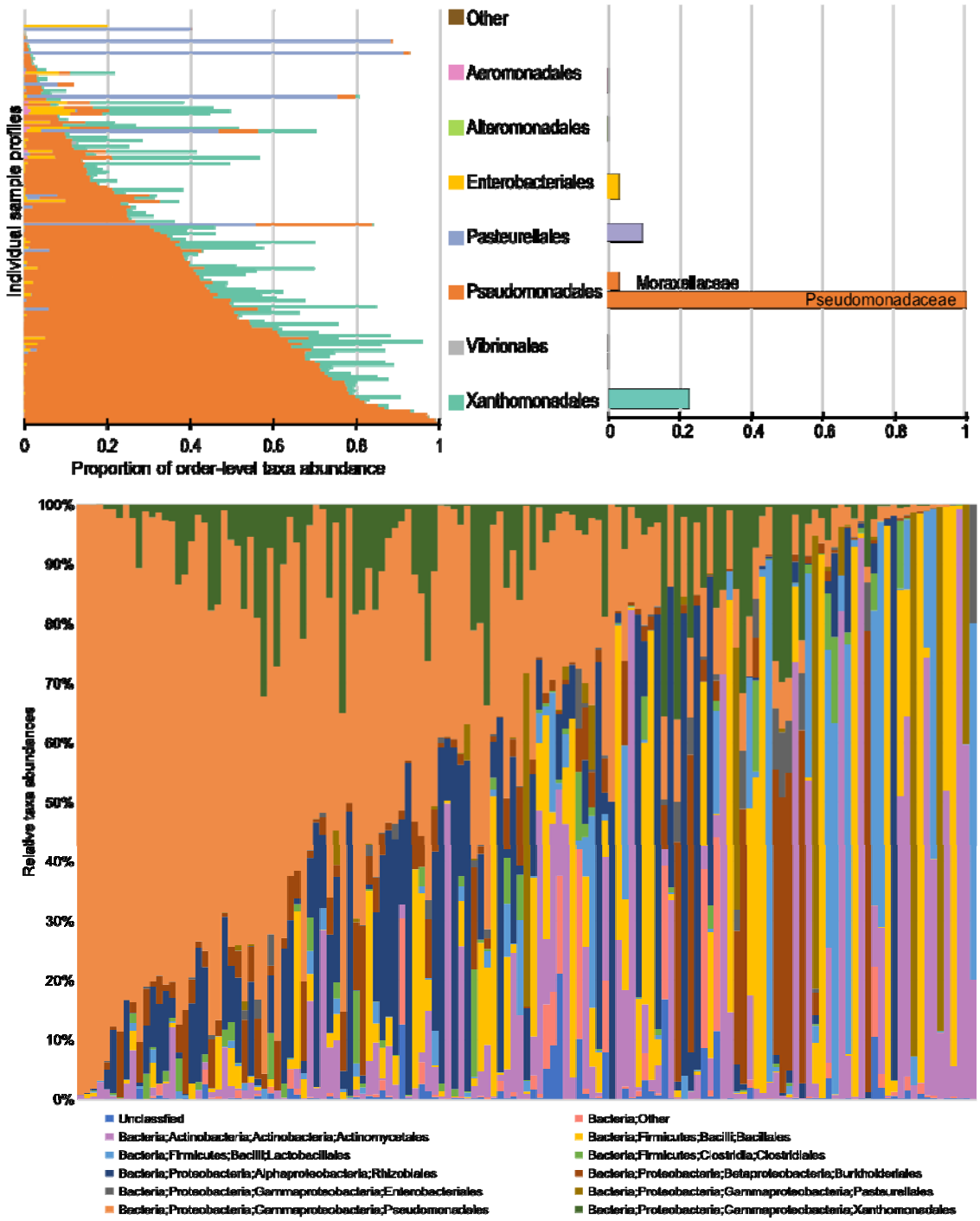

Figure S3. Comprehensive taxonomic breakdown for influenza-infected human subjects. The plot summarizes an order level breakdown of the Gammaproteobacteria observed in infected patients (top left), and the family level classification (top right) for the same, along with the

relative abundances at the **order** level for taxonomic groups that are present in greater than 1% of the samples (bottom).

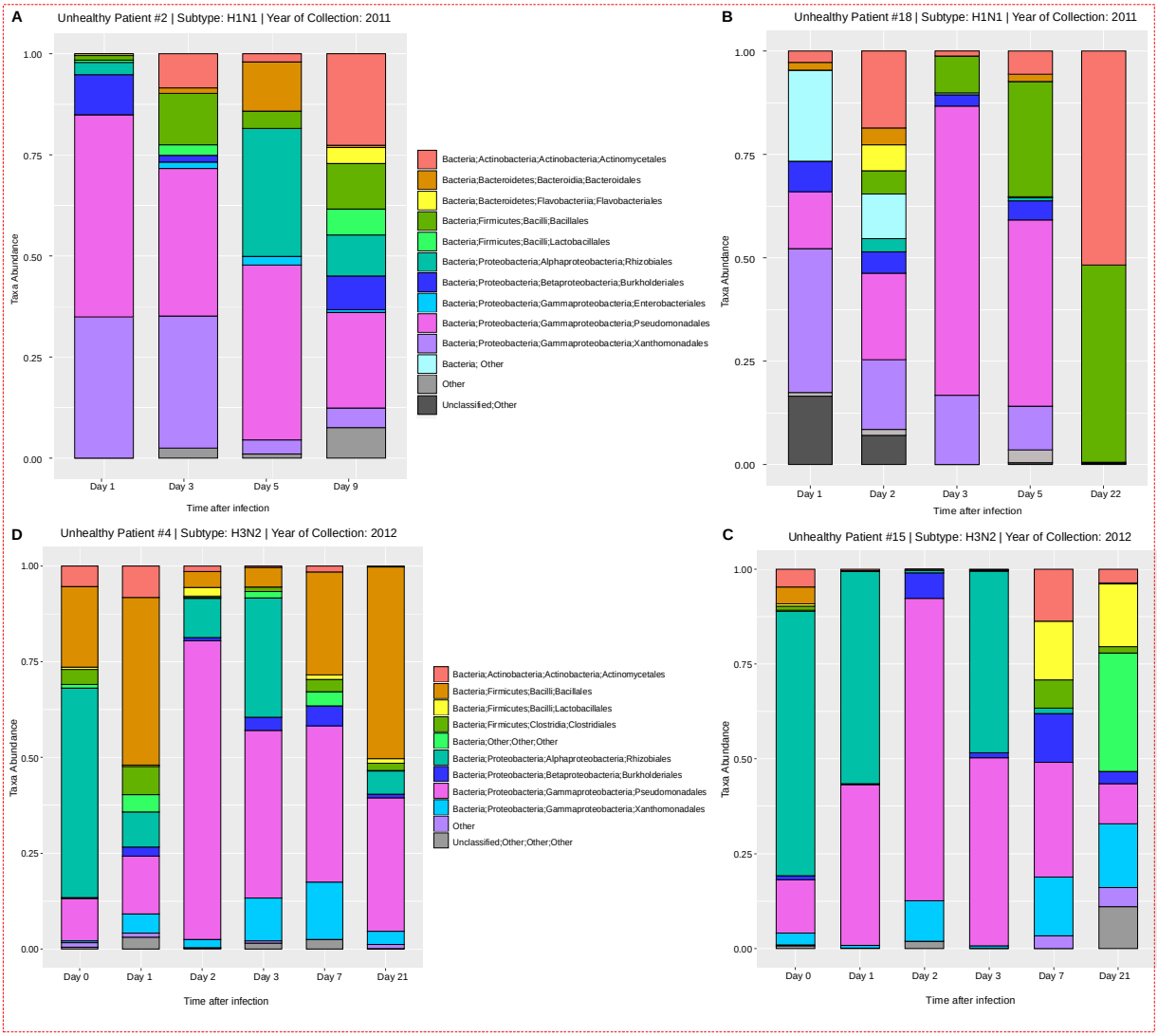
A
Unhealthy Patient #2 | Subtype: H1N1 | Year of Collection: 2011
Taxa Abundance
1.00
0.75
0.50
0.25
0.00
Day 1
Day 3
Day 5
Day 9
Time after infection
Bacteria;Actinobacteria;Actinobacteria;Actinomycetales
Bacteria;Bacteroidetes;Bacteroidia;Bacteroidales
Bacteria;Bacteroidetes;Flavobacteriia;Flavobacteriales
Bacteria;Firmicutes;Bacilli;Bacillales
Bacteria;Firmicutes;Bacilli;Lactobacillales
Bacteria;Proteobacteria;Alphaproteobacteria;Rhizobiales
Bacteria;Proteobacteria;Betaproteobacteria;Burkholderiales
Bacteria;Proteobacteria;Gammaproteobacteria;Enterobacteriales
Bacteria;Proteobacteria;Gammaproteobacteria;Pseudomonadales
Bacteria;Proteobacteria;Gammaproteobacteria;Xanthomonadales
Bacteria; Other
Other
Unclassified;Other
B
Unhealthy Patient #18 | Subtype: H1N1 | Year of Collection: 2011
Taxa Abundance
1.00
0.75
0.50
0.25
0.00
Day 1
Day 2
Day 3
Day 5
Day 22
Time after infection
D
Unhealthy Patient #4 | Subtype: H3N2 | Year of Collection: 2012
Taxa Abundance
1.00
0.75
0.50
0.25
0.00
Day 0
Day 1
Day 2
Day 3
Day 7
Day 21
Time after infection
Bacteria;Actinobacteria;Actinobacteria;Actinomycetales
Bacteria;Firmicutes;Bacilli;Bacillales
Bacteria;Firmicutes;Bacilli;Lactobacillales
Bacteria;Firmicutes;Clostridia;Clostridiales
Bacteria;Other;Other;Other
Bacteria;Proteobacteria;Alphaproteobacteria;Rhizobiales
Bacteria;Proteobacteria;Betaproteobacteria;Burkholderiales
Bacteria;Proteobacteria;Gammaproteobacteria;Pseudomonadales
Bacteria;Proteobacteria;Gammaproteobacteria;Xanthomonadales
Other
Unclassified;Other;Other;Other
C
Unhealthy Patient #15 | Subtype: H3N2 | Year of Collection: 2012
Taxa Abundance
1.00
0.75
0.50
0.25
0.00
Day 0
Day 1
Day 2
Day 3
Day 7
Day 21
Time after infection
E
F

Figure S4. Comprehensive temporal taxonomic breakdown for human subjects. The plot summarizes the relative taxonomic abundances at the order level across all timepoints for taxonomic groups that are present in greater than 1% of the four influenza infected subjects (2 for each virus subtype, A-D clockwise) and 2 healthy subjects (E-F). Pseudomonadales (pink) is prevalent among the infected individuals (to 4), whereas inconsistent taxa are seen among the healthy control individuals (bottom 2).

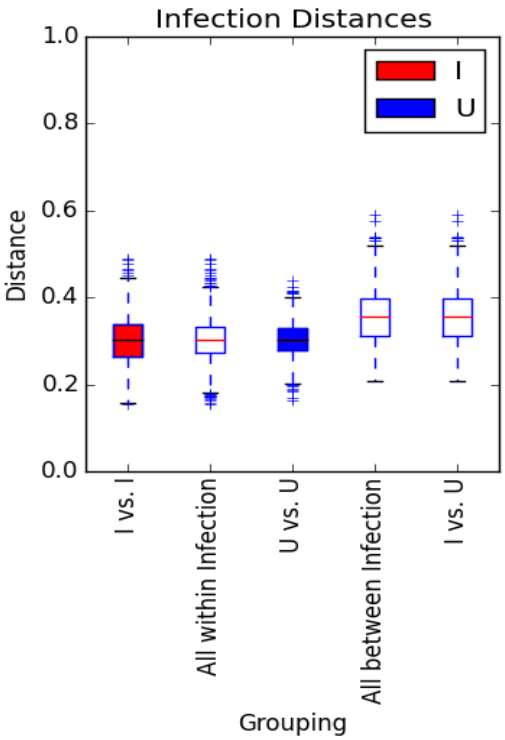

Figure S5. Diversity distance analyses of the microbiome of infected and uninfected ferrets. Box and whisker plots for beta diversity distances within and between influenza types for samples obtained for groups of 7 Infected (I) and 7 Uninfected (U) ferrets. The boxplots represent the diversity between the different infection types. Since there are only two possible infection states for the ferrets, i.e. uninfected and infected, the all-between boxplot is the same as the last boxplot. All the distances were calculated using the Bray-Curtis metric. Red line indicates median in each of the sample groupings and the error bars represent standard deviation.

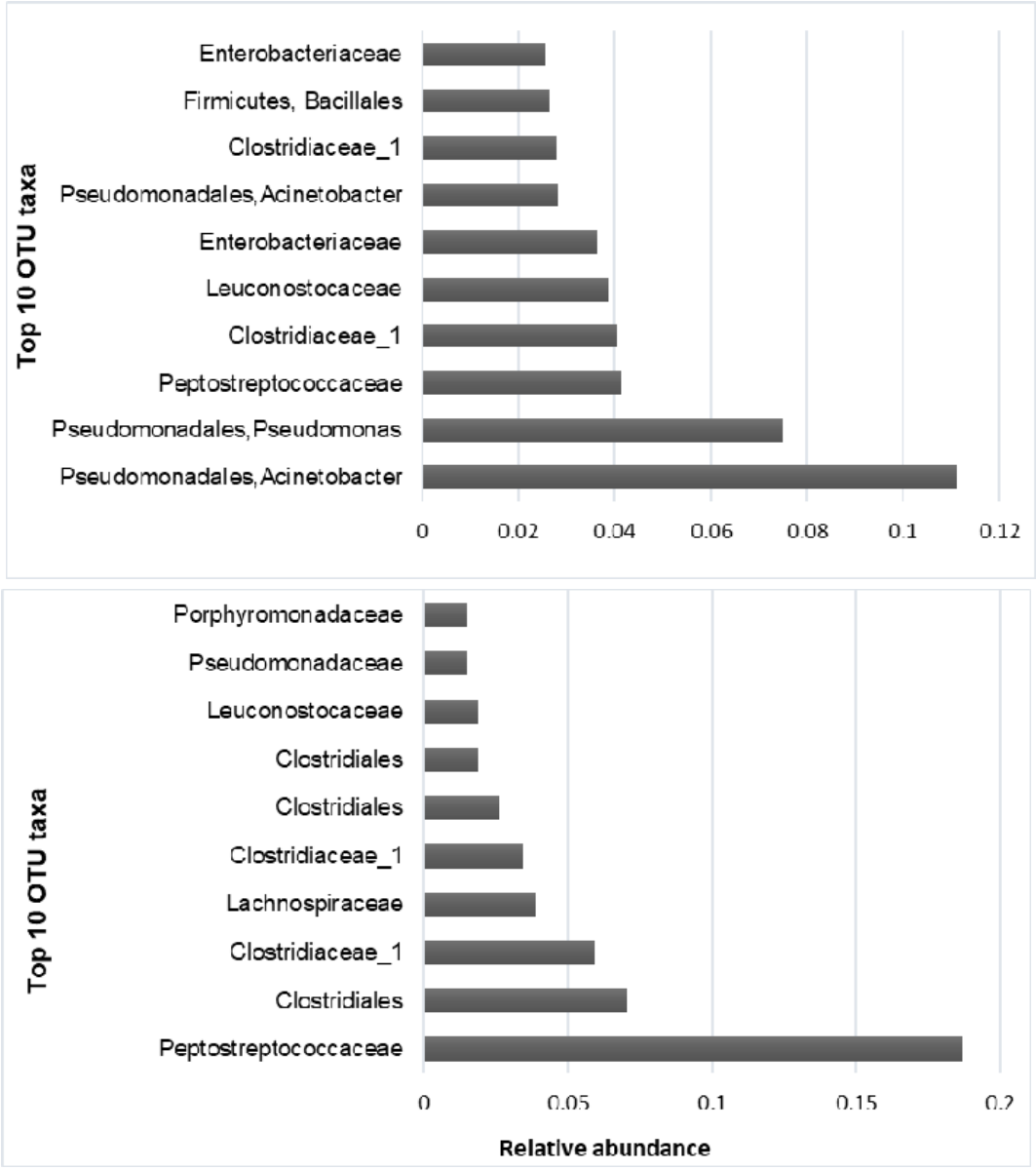

Figure S6. Relative abundance for the top ten most prevalent bacterial families in the URT among infected and uninfected ferrets. The relative abundance was determined based on the Bayesian posterior predictive probabilities from the Infinite Dirichlet multinomial mixture models run over 1000 iterations. Analysis were performed on pyrosequencing data obtained for the V1-V3 region of the 16S rRNA of nasal wash samples obtained from 7 ferrets infected (top) with the A/Netherlands/602/2009 H1N1 virus and from uninfected ferrets (bottom) at the time points indicated on Fig. 4.

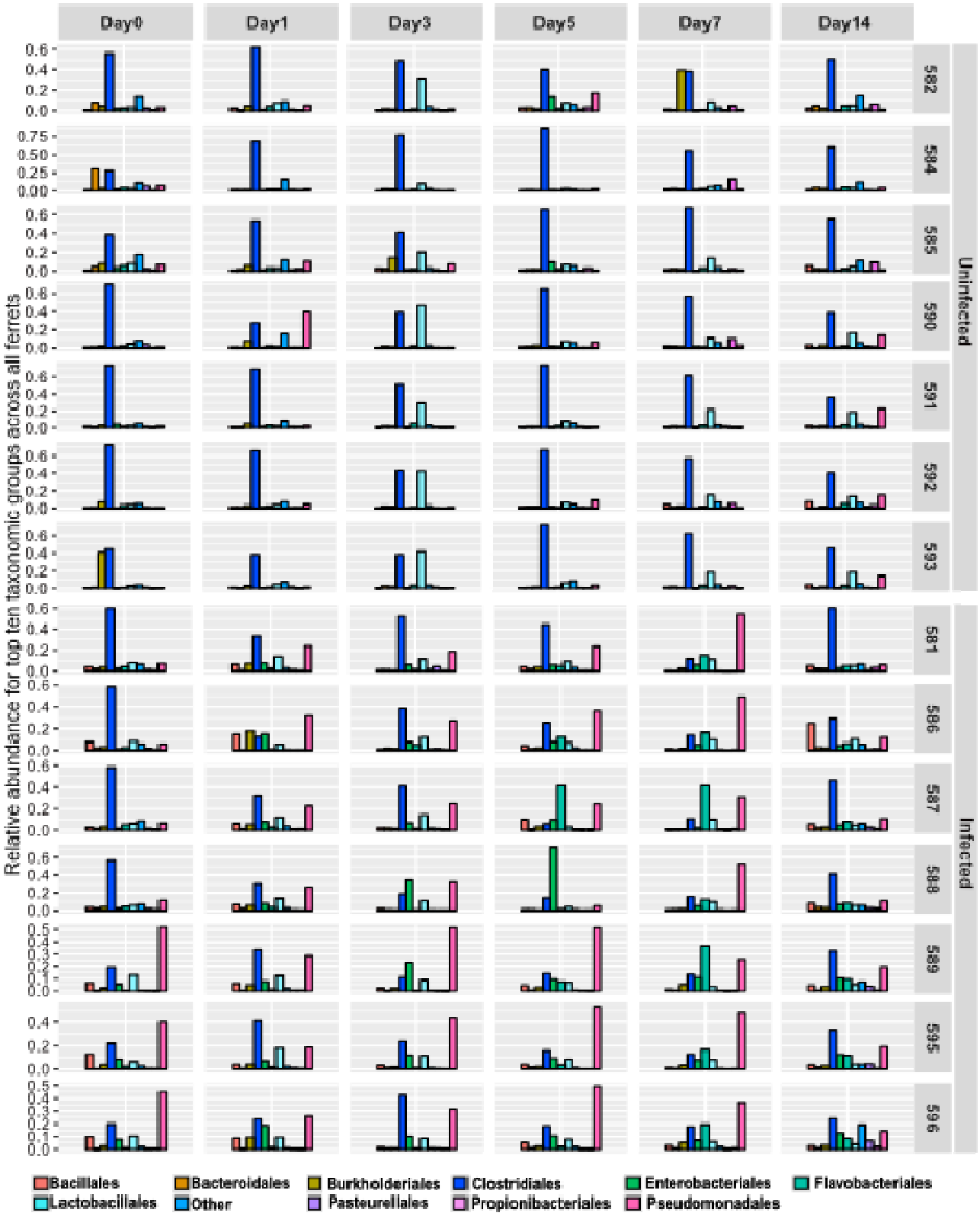
Day0
Day1
Day3
Day5
Day7
Day14
Relative abundance for top ten taxonomic groups across all ferrets
582
584
585
590
591
592
593
581
586
587
588
589
595
596
Uninfected
Infected
Bacillales
Bacteroidales
Burkholderiales
Clostridiales
Enterobacteriales
Flavobacteriales
Lactobacillales
Other
Pasteurellales
Propionibacteriales
Pseudomonadales

855

Figure S7. Comprehensive taxonomic breakdown for all 14 ferrets. The plot summarizes the relative taxonomic abundances at the order level across all timepoints for taxonomic groups that are present in greater than 5% of the samples (see legend below). *Pseudomonadales* (pink) is prevalent among the infected ferrets (bottom 7), whereas Clostridiales (dark blue) is the most abundant among uninfected ferrets (top 7).

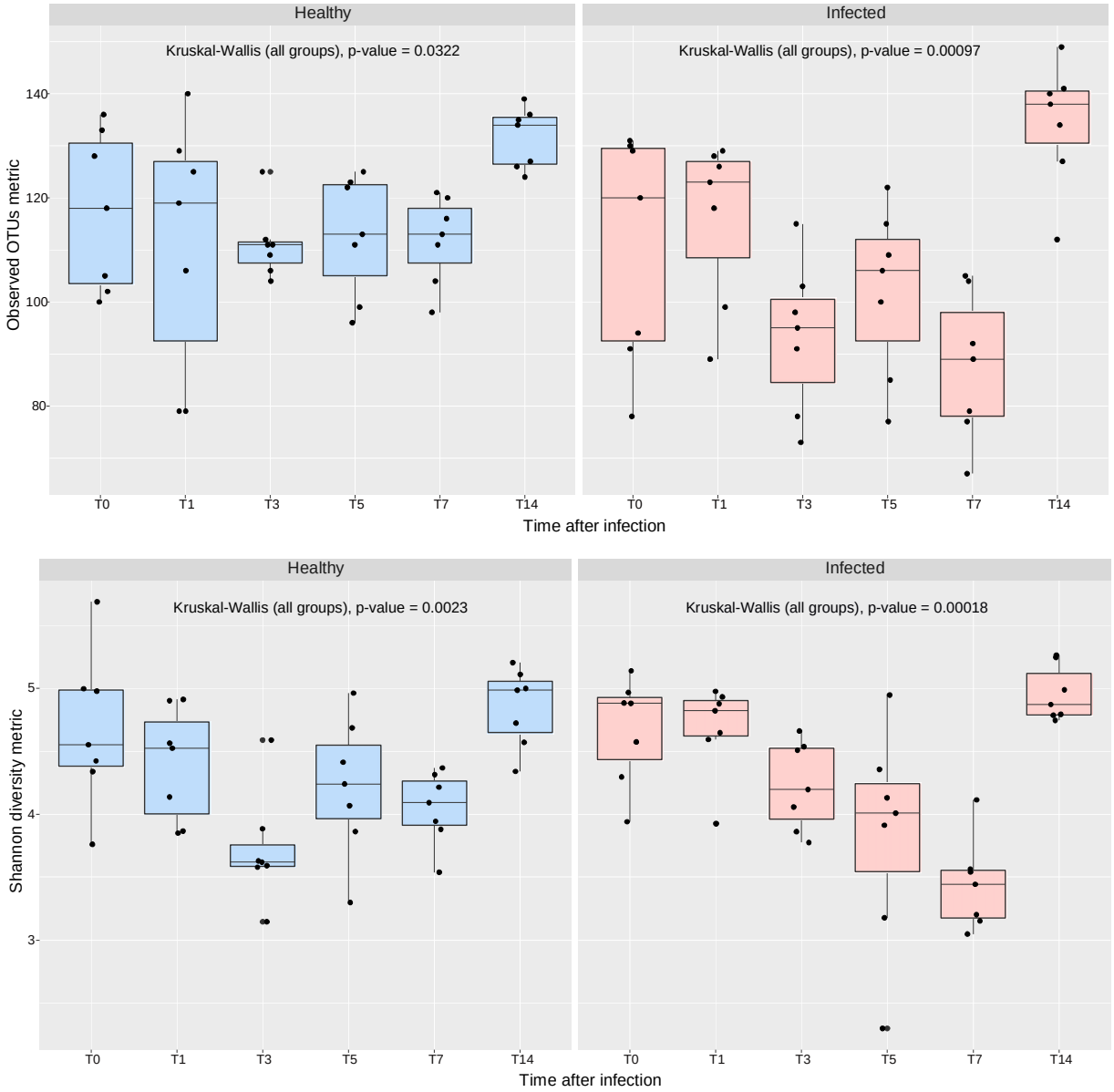

Figure S8. Temporal diversity distance analyses of the microbiome of infected and uninfected ferrets. Changes in alpha diversity within the uninfected (blue) and infected (red) ferrets during IAV infection. A decrease in alpha diversity was observed among the infected animals during the acute phase of viral infection (3 to 7 dpi), with an eventual recovery. This was in agreement with the Pseudomonas bloom observed and the peak IAV titers collected from the same time points. No decreases were observed at any time points for the healthy uninfected group. The boxplots represent the diversity between the different time points. All the distances

were calculated using the Kruskal-Wallis method. The line inside the box indicates median in each of the sample groupings and the error bars represent standard deviation.

Table S1. Clinical-epidemiological characteristics of the hospitalized human patients diagnosed with Influenza A-like illness, and healthy controls.

Characteristic	Hospitalized patients			Healthy controls (n=22)
	Total (n=30)	H1N1 positive (n=13)	H3N2 positive (n=15)	
Age				
< 2 years	2	1	1	0
2 - 65 years	17	8	8	22
> 65 years	11	4	6	0
Gender				
Male	15	7	7	10
Female	15	6	8	12
Clinical severity factors				
Hospitalized by Influenza	23	8	13	N/A
CCU by Infuenza	11	5	6	N/A
O2 supply	20	8	10	N/A
MV supply	7	5	1	N/A
VAD supply	5	4	1	N/A
Treatments				
Antibiotics	27	12	13	N/A
Antiviral	29	12	15	N/A
Comorbidities				
Asthma	2	0	2	N/A
COPD/Respiratory pediatric disease	3	2	1	N/A
Diabetes	8	3	4	N/A
Obesity	7	3	4	N/A
Cancer	4	3	1	N/A
Cronical cardiovascular disease	12	5	6	N/A
Cronical renal disease	2	2	0	N/A
Neurological disorder	5	2	3	N/A
Severe inmunological compromise	9	5	4	N/A
Symptoms				
Fever	24	12	10	N/A
Runny nose	20	9	10	N/A
Throat pain	4	1	3	N/A
Expectoration	22	11	10	N/A
Myalgia	16	8	8	N/A
Conjunctivitis	5	5	0	N/A
Nasopharyngeal samples sequenced				
2 days	3	1	0	0
3 days	4	3	0	0
4 days	6	5	0	1
5 days	12	4	8	1
6 days	5	0	5	20
7 days	3	0	2	0
Day up to 21 dpi.	18	1	15	22

CCU: Clinical Care Unit, MV: Mechanical ventilation, VAD: Vasoactive drugs, COPD: Cronical obstructive pulmonary disease. Dpi: Days post infection. N/A: Not applicable.

Table S2. Two-sided Student's two sample t test results for human samples. Comparison of every pair of boxplots (Fig. S1) to determine if they are significantly different from each other. The significance indicates that samples within the same infection state are significantly more similar to each other than samples across or between infection states.

Group 1	Group 2	t statistic	Parametric p-value	Parametric p-value (Bonferroni-corrected)
Flu negative vs. Flu negative	All within Infection	-55.0578521	0	0
Flu negative vs. Flu negative	P vs. P	-75.3610857	0	0
Flu negative vs. Flu negative	P vs. U	-138.6375158	0	0
Flu negative vs. Flu negative	U vs. U	-154.3952941	0	0
Flu negative vs. Flu negative	Flu negative vs. P	-221.0081364	0	0
Flu negative vs. Flu negative	All between Infection	-263.0843447	0	0
Flu negative vs. Flu negative	Flu negative vs. U	-291.4056393	0	0
All within Infection	P vs. P	-21.37412196	8.63E-100	2.42E-98
All within Infection	P vs. U	-52.60214147	0	0
All within Infection	U vs. U	-62.86129962	0	0
All within Infection	Flu negative vs. P	-88.60634085	0	0
All within Infection	All between Infection	-150.8209456	0	0
All within Infection	Flu negative vs. U	-140.7417865	0	0
P vs. P	P vs. U	-4.94665465	7.81E-07	2.19E-05
P vs. P	U vs. U	-8.909094618	6.93E-19	1.94E-17
P vs. P	Flu negative vs. P	-24.73696145	9.46E-129	2.65E-127
P vs. P	All between Infection	-24.68676524	9.22E-133	2.58E-131
P vs. P	Flu negative vs. U	-34.22348208	7.20E-246	2.02E-244
P vs. U	U vs. U	-6.730380217	1.80E-11	5.05E-10
P vs. U	Flu negative vs. P	-29.09777915	4.22E-178	1.18E-176
P vs. U	All between Infection	-35.90792139	1.91E-275	5.35E-274
P vs. U	Flu negative vs. U	-48.51917022	0	0
U vs. U	Flu negative vs. P	-21.754135	1.67E-102	4.68E-101
U vs. U	All between Infection	-27.42974294	2.62E-163	7.34E-162
U vs. U	Flu negative vs. U	-40.12946953	0	0
Flu negative vs. P	All between Infection	0.095133236	0.924209718	1
Flu negative vs. P	Flu negative vs. U	-14.55953211	9.70E-48	2.72E-46
All between Infection	Flu negative vs. U	-19.42583244	1.35E-83	3.77E-82

Table S3. Non-parametric multivariate analysis using Anosim and Adonis tests. Examining the effect of clinical parameters (gender, age and antibiotic usage) on the infected human URT microbiomes.

Variable	**Anosim test** (*permutations=999*)	**df** *(n-1)*	**Adonis test** (*permutations=999*)	**df** *(n-1)*
Gender (n=2; M/F)	R statistic= 0.03124 p-value < 0.023	1	R^2 statistic= 0.0209 p-value < 0.003	1
Antibiotic Usage (n=2; Y/N)	R statistic= -0.046 p-value < 0.732	1	R^2 statistic= 0.01216 p-value < 0.043	1
Age (n=26)	R statistic= 0.4778 p-value < 0.001	25	R^2 statistic= 0.409 p-value < 0.001	25

Table S4: Random forest analysis results for the human microbiomes. Ranks range from the first few attributes predictive of the infection state, followed by the attributes that are most predictive of the data (maximum accuracy).

Rank (1-667)	**Ranked attributes (OTUs)**	**OTU taxonomy**	**Accuracy (%)**
1st	**Otu000002**	Bacteria;Proteobacteria; Gammaproteobacteria; Pseudomonadales	64.00
2nd	Otu000002; **Otu000001**	Bacteria;Proteobacteria; Alphaproteobacteria; Rhizobiales; Brucellaceae; Ochrobactrum	64.00
3rd	Otu000002; Otu000001; **Otu000003**	Bacteria; Proteobacteria; Gammaproteobacteria; Pseudomonadales; Pseudomonadaceae; Pseudomonas	62.00
137th	Otu000002; Otu000001; Otu000003; Otu000006; Otu000055; Otu000035; Otu000005, etc (130 other OTUs)		**71.00**

Table S5. Two-sided Student's two sample t test results for ferrets. Comparison of every pair of boxplots (Fig. S4). The significance indicates that samples within the same infection state are significantly more similar to each other than samples across or between infection states.

Group 1	Group 2	t statistic	Parametric p-value	Parametric p-value (Bonferroni-corrected)
I vs. I	All within Infection	0.073562	0.941364778	1
I vs. I	U vs. U	0.133209	0.894043353	1
I vs. I	All between Infection	-22.1458	9.17E-100	9.17E-99
I vs. I	I vs. U	-22.1458	9.17E-100	9.17E-99
All within Infection	U vs. U	0.080792	0.935613791	1
All within Infection	All between Infection	-29.1592	1.90E-167	1.90E-166
All within Infection	I vs. U	-29.1592	1.90E-167	1.90E-166
U vs. U	All between Infection	-23.8123	1.24E-113	1.24E-112
U vs. U	I vs. U	-23.8123	1.24E-113	1.24E-112
All between Infection	I vs. U	0	1	1

Table S6. Random forest analysis results for the ferret microbiomes. Ranks range from the first few attributes predictive of the infection state, followed by the attributes that are most predictive of the data (maximum accuracy).

Rank (1-259)	**Ranked attributes (OTUs)**	**OTU taxonomy**	**Accuracy (%)**
1st	**Otu000004**	Bacteria;Proteobacteria; Gammaproteobacteria; Pseudomonadales; Moraxellaceae;Acinetobacter	79.79
2nd	Otu000004; **Otu000028**	Bacteria;Proteobacteria; Gammaproteobacteria; Enterobacteriales; Enterobacteriaceae;Enterobacter	91.69
3rd	Otu000004; Otu000028; **Otu000017**	Bacteria;Firmicutes; Bacilli;Bacillales; Family_XII;Exiguobacterium	89.26
7th	Otu000004; Otu000028; Otu000017; Otu000001; Otu000027; Otu000170; Otu000008		**96.47**